NASA/TM—2019-220029

Ruggedness Evaluation of ASTM International Standard Test Methods for Shape Memory Materials: E3097 Standard Test Method for Mechanical Uniaxial Constant Force Thermal Cycling of Shape Memory Alloys

Othmane Benafan, Glen S. Bigelow, and Leo Wood
Glenn Research Center, Cleveland, Ohio

February 2019

NASA STI Program . . . in Profile

Since its founding, NASA has been dedicated to the advancement of aeronautics and space science. The NASA Scientific and Technical Information (STI) Program plays a key part in helping NASA maintain this important role.

The NASA STI Program operates under the auspices of the Agency Chief Information Officer. It collects, organizes, provides for archiving, and disseminates NASA's STI. The NASA STI Program provides access to the NASA Technical Report Server—Registered (NTRS Reg) and NASA Technical Report Server—Public (NTRS) thus providing one of the largest collections of aeronautical and space science STI in the world. Results are published in both non-NASA channels and by NASA in the NASA STI Report Series, which includes the following report types:

- TECHNICAL PUBLICATION. Reports of completed research or a major significant phase of research that present the results of NASA programs and include extensive data or theoretical analysis. Includes compilations of significant scientific and technical data and information deemed to be of continuing reference value. NASA counter-part of peer-reviewed formal professional papers, but has less stringent limitations on manuscript length and extent of graphic presentations.

- TECHNICAL MEMORANDUM. Scientific and technical findings that are preliminary or of specialized interest, e.g., "quick-release" reports, working papers, and bibliographies that contain minimal annotation. Does not contain extensive analysis.

- CONTRACTOR REPORT. Scientific and technical findings by NASA-sponsored contractors and grantees.

- CONFERENCE PUBLICATION. Collected papers from scientific and technical conferences, symposia, seminars, or other meetings sponsored or co-sponsored by NASA.

- SPECIAL PUBLICATION. Scientific, technical, or historical information from NASA programs, projects, and missions, often concerned with subjects having substantial public interest.

- TECHNICAL TRANSLATION. English-language translations of foreign scientific and technical material pertinent to NASA's mission.

For more information about the NASA STI program, see the following:

- Access the NASA STI program home page at http://www.sti.nasa.gov

- E-mail your question to help@sti.nasa.gov

- Fax your question to the NASA STI Information Desk at 757-864-6500

- Telephone the NASA STI Information Desk at 757-864-9658

- Write to:
  NASA STI Program
  Mail Stop 148
  NASA Langley Research Center
  Hampton, VA 23681-2199

NASA/TM—2019-220029

Ruggedness Evaluation of ASTM International Standard Test Methods for Shape Memory Materials: E3097 Standard Test Method for Mechanical Uniaxial Constant Force Thermal Cycling of Shape Memory Alloys

Othmane Benafan, Glen S. Bigelow, and Leo Wood
Glenn Research Center, Cleveland, Ohio

National Aeronautics and
Space Administration

Glenn Research Center
Cleveland, Ohio 44135

February 2019

Acknowledgments

Funding from the NASA Aeronautics Research Mission Directorate (ARMD) Transformational Tools and Technologies (TTT) project is gratefully acknowledged. The authors also acknowledge contributions from the Aerospace Vehicle Systems Institute (AVSI) members.

This work was sponsored by the
Transformative Aeronautics Concepts Program.

Trade names and trademarks are used in this report for identification only. Their usage does not constitute an official endorsement, either expressed or implied, by the National Aeronautics and Space Administration.

Level of Review: This material has been technically reviewed by technical management.

Available from

NASA STI Program
Mail Stop 148
NASA Langley Research Center
Hampton, VA 23681-2199

National Technical Information Service
5285 Port Royal Road
Springfield, VA 22161
703-605-6000

This report is available in electronic form at http://www.sti.nasa.gov/ and http://ntrs.nasa.gov/

Ruggedness Evaluation of ASTM International Standard Test Methods for Shape Memory Materials: E3097 Standard Test Method for Mechanical Uniaxial Constant Force Thermal Cycling of Shape Memory Alloys

Othmane Benafan, Glen S. Bigelow, and Leo Wood*
National Aeronautics and Space Administration
Glenn Research Center
Cleveland, Ohio 44135

Summary

This paper evaluates the ruggedness testing of the newly released ASTM International E3097 Standard Test Method for Mechanical Uniaxial Constant Force Thermal Cycling of Shape Memory Alloys. The ruggedness experiment was designed with eight runs in two replicates, consisting of seven factors of strain rate ($\dot{e}$), heating and cooling rates ($\dot{T}_{heat}$ and $\dot{T}_{cool}$, respectively), upper and lower cycle temperatures (*UCT* and *LCT*, respectively), hold time (t_{hold}), and minimum load (F_{min}) imparted on the samples. The results indicate that the hold time factor had no effect on any result variable. The minimum load factor, alternatively, had the greatest effect on several result variables, with the greatest influence on the strains at martensite start and finish (strain variation ~0.1 percent), and the strains at the upper and lower cycle temperatures (strain variation of 0.14 percent). The *UCT* was found to have a large effect on the austenite and martensite finish tangent line and data intersect, denoted by A_f* and M_f*, by ~17 and 4 °C, respectively. The testing methodology, analysis techniques, and resulting conclusions on the ruggedness of the test methods are presented.

1.0 Introduction

Shape memory alloy (SMA) actuator properties have been measured and reported for hundreds of alloy systems, yet not in any comprehensive or standardized format. Given their complex behavior and numerous dependent factors, having a standardized and robust method to consistently produce and interpret SMA data can be very beneficial. Initial efforts to address this lack of test methods was spearheaded by the Consortium for the Advancement of Shape Memory Alloy Research and Technology (CASMART) established in 2007 (Ref. 1). Several contributions flourished from this effort and laid the groundwork for several aspects of property measurement, test and analysis methods, and nomenclature, among others. In 2015, a collaborative effort composed of international members from industry and government was formed to build on this prior work and develop the first-ever material specification and test standards for SMA actuators. The team was organized through the Aerospace Vehicle Systems Institute (AVSI) with the purpose of identifying, developing, and disseminating SMA test methods with an established standards development organization (Ref. 2).

Recently, two newly developed ASTM International test methods for SMA materials and components were released to the public. These standards, listed as E3097 Standard Test Method for Mechanical Uniaxial Constant Force Thermal Cycling of Shape Memory Alloys (UCFTC) (Ref. 3) and E3098

*Summer intern in Lewis' Educational and Research Collaborative Internship Project (LeRCIP), undergraduate at Texas A&M University.

Standard Test Method for Mechanical Uniaxial Pre-strain and Thermal Free Recovery of Shape Memory Alloys (Ref. 4), represent a critical step toward the commercialization and production of SMA actuators. While several other standards exist based primarily on the superelastic response (for the medical industry) (Refs. 5 to 9), these two standards represent the very first universally accepted standards that define procedures for measuring shape memory effect properties, such as transformation temperatures, strains, and stiffness related to SMA thermoelastic actuators.

As with most ASTM standards, it is imperative to evaluate the sensitivity of these methods and ensuing significances. The methods define procedures with method parameters and factors that could influence the test results. These parameters and their suggested values were initially selected based on prior members' experiences to provide guidance and a starting point. Thus, the goal of this work is to perform ruggedness tests on the first test method (E3097) by using controlled experiments in which factors are deliberately varied. Such a test is performed before executing a larger interlaboratory study, mainly to anticipate and/or eliminate potential sources of inaccuracies as well as to determine the level of measured property variation due to the method parameters, aside from material or operator variations (inconsistencies). In conjunction with the AVSI team, a seven-factor ruggedness experiment was designed with eight runs in two replicates. The selected factors were strain rate ($\dot{e}$), heating and cooling rates ($\dot{T}_{heat}$ and $\dot{T}_{cool}$, respectively), upper and lower cycle temperatures (*UCT* and *LCT*, respectively), hold time (t_{hold}), and minimum load (F_{min}) imparted on the samples. Testing is performed at five different organizations on three material forms, including rods, wires, and flat sheets, all of which are critical to SMA actuator applications. Ruggedness test calculations were performed in accordance with established methods (Ref. 10) in addition to other approaches that were used to further examine the SMA behavior. The testing methodology, analysis techniques, and resulting conclusions on the ruggedness of the E3097 test method are presented. The work reported here is limited to tests conducted at the NASA Glenn Research Center that used round dogbone specimens (rod form).

2.0 Experimental Methods

2.1 Material

The material used in this study was a binary NiTi alloy with nominal composition of 55.3Ni-44.7Ti wt% produced by ATI Specialty Alloys and Components (heat #836441). Cylindrical, dogbone specimens, with gage dimensions of 3.81 mm (0.15 in.) in diameter and 19.05 mm (0.75 in.) in length, were machined from a hot-rolled rod and subjected to an annealing heat treatment. Stress-free transformation temperatures were measured by using differential scanning calorimetry (DSC), as shown in Figure 1, and were found to be 77, 96, 67, and 50 °C, for austenite start (A_s), austenite finish (A_f), martensite start (M_s), and martensite finish (M_f), respectively.

2.2 Thermomechanical Testing

Thermomechanical tests were performed on an MTS 810 servohydraulic load frame (MTS Systems Corporation) equipped with an MTS FlexTest® SE digital controller, a Eurotherm® 3504 temperature controller (Schneider Electric), and an Ameritherm NovaStar 7.5-kW induction heater (Ambrell Corporation). A type-K thermocouple was spot welded directly to the midpoint of the sample gage section and used to measure temperature. Strain measurements were made by using an MTS 632.53E–14 high-temperature extensometer fitted with alumina rods and having a gage length of 12.7 mm (0.5 in.).

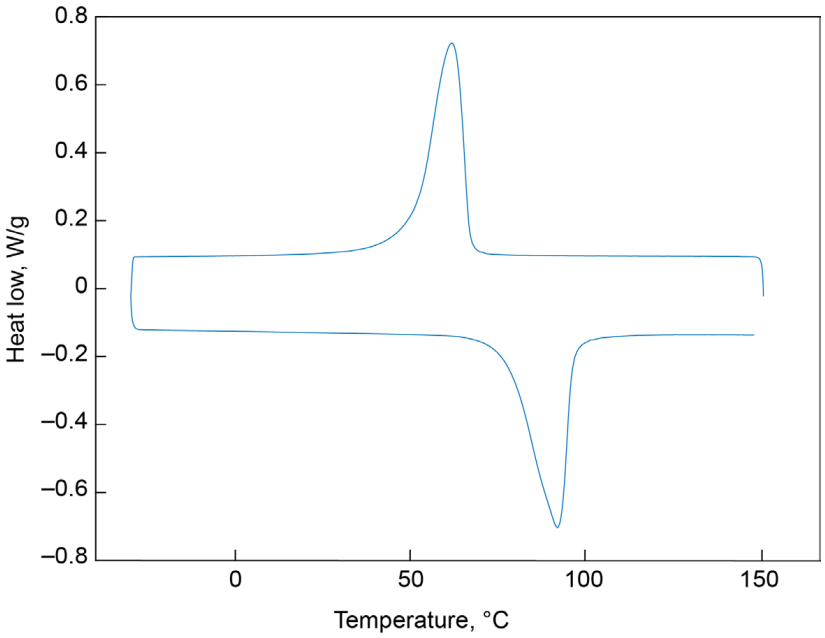

Figure 1.—Differential scanning calorimetry response of 55.3Ni-44.7Ti wt% shape memory alloy tested.

2.3 Test Procedure

Testing was performed in accordance with the test procedures outlined in the ASTM E3097 test methods (Ref. 3) and only a brief summary is provided here. The UCFTC test consists of thermomechanically cycling an SMA under an applied axial stress to determine transformation temperatures, related transformation strains, and the residual strains. The initial step consists of a normalization phase where the specimen is mounted on the load frame at room temperature and held under a minimum load not to exceed 7 MPa (~1 ksi). The specimen is then heated to the upper cycle temperature (*UCT*), cooled to the lower cycle temperature (*LCT*), and then reheated and held at the *UCT* for a specified time (hold time). This normalization procedure is performed to alleviate any residual stresses that may have arisen from sample handling, such as during machining or mounting operations. After normalization, the specimen is loaded to the selected stress level at *UCT*, followed by cooling and heating between the designated lower and upper cycling temperatures, with holds at both to ensure equilibration of temperature and/or strain. This procedure is schematically illustrated in Figure 2 along with the associated test result variables.

2.4 Experiment Design

The fractional factorial test design and accompanying statistical analysis methods used are performed in accordance with the standard practice for ruggedness tests outlined by ASTM standard E1169 (Ref. 10). The seven factors and their associated level settings are shown in Table I. The selected factors, $\dot{e}$, $\dot{T}_{heat}$, $\dot{T}_{cool}$, *UCT*, *LCT*, t_{hold}, and F_{min}, are believed to have the highest potential to affect the results. For each factor, the level settings, indicated by either (–1) or (+1) for low or high levels, respectively, were chosen to encompass the limits that could be expected to exist between different laboratories with different types of test equipment and control limitations.

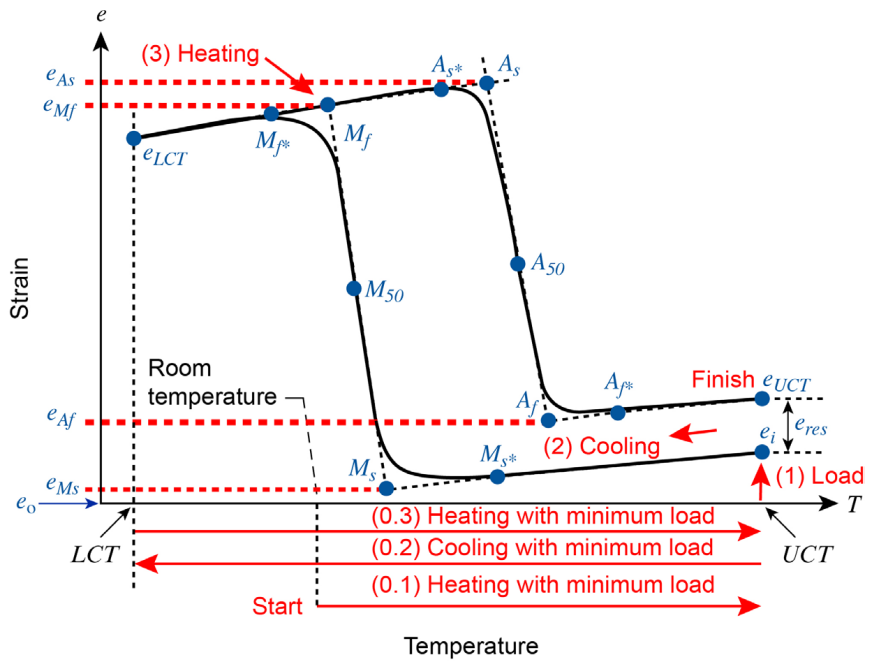

Figure 2.—Constant force thermal cycle and associated test parameters (adopted from Ref. 3). Normalization step is outlined at bottom of sketch labeled as “heating/cooling with minimum load”. Where A_{50} is austenite 50 percent, A_f is austenite finish, A_f* is austenite finish tangent line and data intersect, A_s is austenite start, A_s* is austenite start tangent line and data intersect, e is strain, e_0 is initial strain (at upper cycle temperature (*UCT*) after normalizing), e_{Af} is strain at austenite finish temperature (fit line intersection point), e_{As} is strain at austenite start temperature (fit line intersection point), e_i is initial loading strain (at *UCT*, at load), e_{LCT} is strain at lower cycle temperature (*LCT*) (after cooling under load), e_{Mf} is strain at martensite finish temperature (fit line intersection point), e_{Ms} is strain at martensite start temperature (fit line intersection point), e_{UCT} is strain at upper cycle temperature (after cooling under load), M_{50} is martensite 50 percent, M_f is martensite finish, M_f* is martensite finish tangent line and data intersect, M_s is martensite start, M_s* is martensite start tangent line and data intersect, and T is temperature.

TABLE I.—RUGGEDNESS TEST FACTORS AND LEVEL SETTINGS

Level	A	B	C	D	E	F	G
	Strain rate, $\dot{e}$	Cooling rate, $\dot{T}_{cool}$	Heating rate, $\dot{T}_{heat}$	Upper cycle temperature, *UCT*	Lower cycle temperature, *LCT*	Hold time, t_{hold}	Minimum load, F_{min}
–1	0.001 mm/mm per min	1 °C/min	1 °C/min	150 °C	25 °C	30 s	1 MPa
+1	0.01 mm/mm per min	4 °C/min	4 °C/min	180 °C	37 °C	600 s	7 MPa
Run no.	Level setting						
1, 9	+1	+1	+1	–1	+1	–1	–1
2, 10	–1	+1	+1	+1	–1	+1	–1
3, 11	–1	–1	+1	+1	+1	–1	+1
4, 12	+1	–1	–1	+1	+1	+1	–1
5, 13	–1	+1	–1	–1	+1	+1	+1
6, 14	+1	–1	+1	–1	–1	+1	+1
7, 15	+1	+1	–1	+1	–1	–1	+1
8, 16	–1	–1	–1	–1	–1	–1	–1

3.0 Analysis Methods

All raw data files were reduced and tabulated on a standardized format as defined by the AVSI team per ASTM E3097 (see Appendix B). These data were reduced by a single analyst using Glenn's SMA analyses tools based on tangent line fits, as partially outlined in References 8 and 11. Analysis of the statistical significance and relative importance of the seven different factors was performed by using both half-normal plots and a student's two-tailed *t*-test (Ref. 10). The half-normal plot allows for approximate grouping of factors as important or unimportant for influencing a chosen result in addition to ranking factors by their relative importance. These plots also provide a visual metric of whether a factor's effect falls within the normal scatter of data or provides a real influence. Referring back to Reference 10, the half-normal plots were constructed based on two main quantities: the main effect of each factor on the selected result variable and the standard error of effects from all trials. The main effect of each factor is determined from the average results of all the high (+1) and the low (–1) levels by using Equation (1) as follows:

$$effect = (Ave+) - (Ave-) \tag{1}$$

The estimate of the standard error of an effect, denoted by S_{effect}, is given by

$$S_{effect} = \sqrt{\frac{4s_{rep}^2}{N \cdot reps}} \tag{2}$$

where N is the number of runs (i.e., $N = 8$) in the experiment design, *reps* is the number of replicates (i.e., *reps* = 2), and s_{rep} is the estimated standard deviation (STDEV) of the test results given by

$$s_{rep} = \frac{s_d}{\sqrt{2}} \tag{3}$$

where s_d is the STDEV of the differences between replicates 1 and 2, with each difference calculated as rep. 2 – rep. 1. An example calculation used to construct a half-normal plot is shown in Table II for the SMA property, A_f. In this example, the STDEV of the differences s_d is calculated as STDEV (–0.657, 0.482, –0.555, –0.593, 0.475, –2.25, –0.068, –1.668) = 0.962.

From these values, the effects of all factors can be ranked and assigned half-normal distribution plotting values, which are predetermined from a half-normal distribution for the seven factors (Ref. 10). This ranking, along with the half-normal plotting values obtained from Table A2.1 in Reference 10, are shown in Table III. These plotting values will comprise the y-coordinates for each factor in the half-normal plot.

TABLE II.—RUGGEDNESS EXAMPLE CALCULATIONS
FOR AUSTENITE FINISH, A_f, RESULTS

Run no.	Strain rate, $\dot{e}$	Cooling rate, $\dot{T}_{cool}$	Heating rate, $\dot{T}_{heat}$	Upper cycle temperature, *UCT*	Lower cycle temperature, *LCT*	Hold time, t_{hold}	Minimum load, F_{min}	Rep. 1	Rep. 2	Replicates (Reps.) 1 and 2	
	A	B	C	D	E	F	G	Result	Result	Average	Difference
1	+1	+1	+1	–1	+1	–1	–1	122.876	122.219	122.548	–0.657
2	–1	+1	+1	+1	–1	+1	–1	121.800	122.282	122.041	0.482
3	–1	–1	+1	+1	+1	–1	+1	123.753	123.198	123.476	–0.555
4	+1	–1	–1	+1	+1	+1	–1	127.098	126.505	126.802	–0.593
5	–1	+1	–1	–1	+1	+1	+1	122.374	122.849	122.612	0.475
6	+1	–1	+1	–1	–1	+1	+1	124.048	121.798	122.923	–2.250
7	+1	+1	–1	+1	–1	–1	+1	123.267	123.199	123.233	–0.068
8	–1	–1	–1	–1	–1	–1	–1	125.214	123.546	124.380	–1.668
+1 average	124.0248	122.6082	122.7467	123.8877	123.8950	123.5943	123.0607	STDEV[a] of differences between replicates 1 and 2, s_d			0.962
–1 average	122.8289	124.3950	124.2565	123.1155	123.1442	123.4090	123.9425	Estimated STDEV of test results, s_{rep}			0.680
Effect	1.1960	–1.7868	–1.5098	0.7723	0.7147	0.1853	–0.8817	Standard error of an effect, S_{effect}			0.340

[a]Standard deviation.

TABLE III.—FACTOR RANKINGS AND CALCULATED VALUES
FOR EFFECTS ON AUSTENITE FINISH, A_f

Factor ranking	Factor	Effect	Student's *t*-value[a]	*p-value*,[b] percent	Half-normal plotting values (Ref. 10)
7	B	–1.7868	–5.2537	0.12	1.803
6	C	–1.5098	–4.4392	0.30	1.242
5	A	1.1960	3.5165	0.98	0.921
4	G	–0.8817	–2.5924	3.58	0.674
3	D	0.7723	2.2708	5.74	0.464
2	E	0.7147	2.1014	7.37	0.272
1	F	0.1853	0.5448	60.28	0.090

[a]See Reference 10.
[b]Probability.

Also reported in Table III are the Student's *t*-value (see Ref. 10) and the associated *p-values*. These are used to judge the probability of a null hypothesis being valid. In other words, based on the assumption that a factor has no effect, the probability of a given *t*-score occurring is determined. If this probability, or *p-value*, is less than 5 percent, then the factor can be said to have some effect within a 95 percent confidence interval. The *p-value* for each factor is a function of both the *t*-score for the given factor and the degrees of freedom, ν, for the entire experiment. These two values are given by the expressions

$$t = effect \Big/ S_{effect} \tag{4}$$

and

$$\nu = (N-1)(reps-1) \tag{5}$$

The *p-value* is then calculated by using conventional expressions such as the incomplete beta function $I_x(z,w)$ given by

$$p = I_{\left(\nu/\nu+t^2\right)}\left(\frac{\nu}{2},\frac{1}{2}\right) \tag{6}$$

The final aspect used in the half-normal plots of this work is the replicate error line, intended to provide a visual metric of the replicate error present in the experiment. Following ASTM E1169, the replicate error line was calculated by using

$$y = \frac{x}{S_{effect}} \tag{7}$$

An example half-normal plot for the result variable A_f is shown in Figure 3. On the *x*-axis, the absolute value of each factor's effect is plotted, and on the *y*-axis, the half-normal distribution plotting values previously shown in Table III are plotted. Half-normal plots allow for an understanding of what factors may be considered significant or relevant as well as providing a relative ranking of how factors affect a given result variable. The greater the effect of a factor, the farther right it will fall, and the greater the effect relative to other factors observed, the higher it will be placed, meaning that the farther a factor falls from the origin, the more likely it is to have an effect on the result variable. Additionally, the replicate error line provides a quick visual metric for how the effects of a factor compare to the random variation observed across replicates. Anywhere to the left of the line and any effects a factor may have likely fall within the noise observed in the experiment, whereas the farther right of the line a factor falls, the more likely its effect is to be relevant (Figure 3).

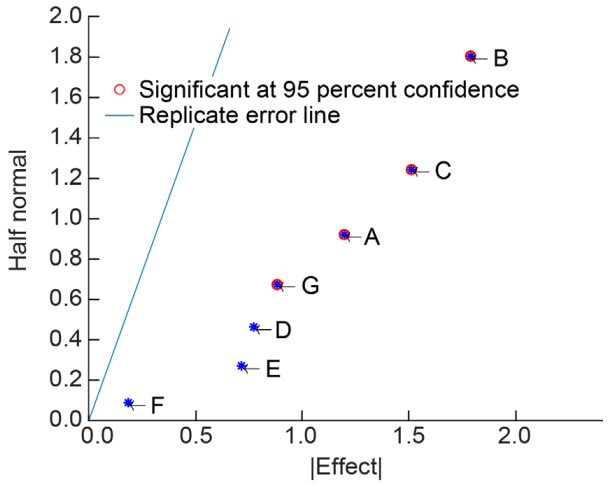

Figure 3.—Example half-normal plot with *t*-test results corresponding to result variable A_f (austenite finish), for factors of A, strain rate; B, cooling rate; C, heating rate; D, upper cycle temperature (*UCT*); E, lower cycle temperature (*LCT*); F, hold time; and G, minimum load.

4.0 Results

4.1 Experiment Factor Verification

As an evaluation of ruggedness is contingent on selected experimental factors varying only between the two settings selected, several runs were analyzed to ensure that the seven factors used were properly maintained at their specific levels. Test equipment and test control methods can play a significant role when evaluating ruggedness. All seven factors were verified in multiple tests and the results of run 3 are presented in this section. Figure 4 shows the strain versus time during the loading and unloading periods where the strain rates are verified. Average slopes of these regions show that strain rate control roughly corresponded to the required value of 0.001 mm/mm/min. Though some fluctuations are present in the initial loading, these are unlikely to affect ruggedness results to any significant degree, and strain rate data for all runs otherwise match the required values closely.

Figure 5 shows the cooling and heating rates. Both cooling and heating rates for run 3 match the required factor values closely, matching the –1 °C/min cooling and +4 °C/min heating rates. This same consistency was found to be true for all runs.

UCT, *LCT*, and hold times followed the required factor values relatively well, as is evident by Figure 6. Despite variation of ~1 °C from *UCT* and *LCT* as well as hold times that are not precisely observed in test data, for all runs, *UCT* and *LCT* were observed to match the required values, and temperature uniformity was maintained during the hold times, to within a reasonable tolerance of ±2 °C.

4.2 Baseline Characterization and Normalization Test

Before conducting the ruggedness tests, preliminary alloy evaluation was conducted on this material lot to observe the nature of the strain-temperature response. Although this is not part of the referred standard, gaining familiarity through these initial baseline tests can better guide the experimental design. Figure 7 illustrates three hysteresis curves obtained at stresses of 100, 200, and 300 MPa. It is apparent that an applied stress of 300 MPa results in very high residual strains while a lower stress of 100 MPa results in a more classical response, which was expected in this untrained material. Thus, a stress of 100 MPa was adopted for the ruggedness evaluation presented in this work.

The normalization test, which is conducted while holding a minimum load not to exceed 7 MPa, is shown in Figure 8. Although the stress is kept at zero, small yet discernable hysteresis curves are developed. This may be due to small internal stresses that could have developed during the material processing or due to the volume change from B2 ⇔ B19′ monoclinic, with the high-temperature B2 phase having a smaller crystallographic volume (Ref. 12).

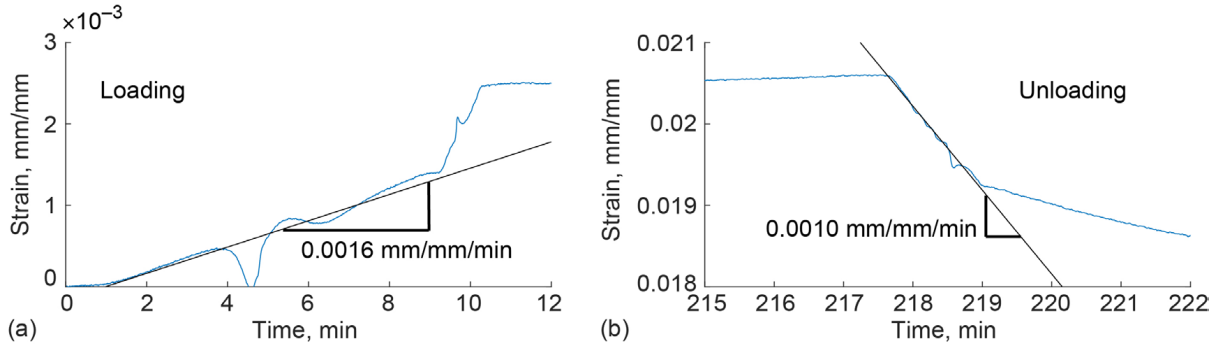

Figure 4.—Strain rate verification: strain versus time corresponding to run 3. (a) Loading. (b) Unloading.

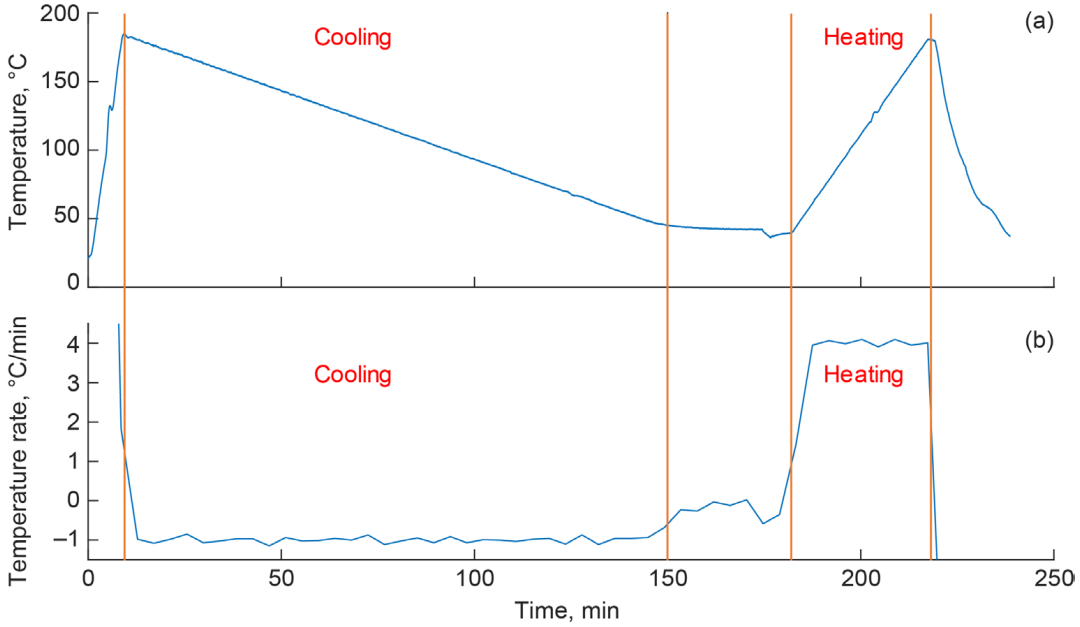

Figure 5.—Cooling and heating rate verification. (a) Temperature versus time. (b) Temperature rate versus time corresponding to run 3.

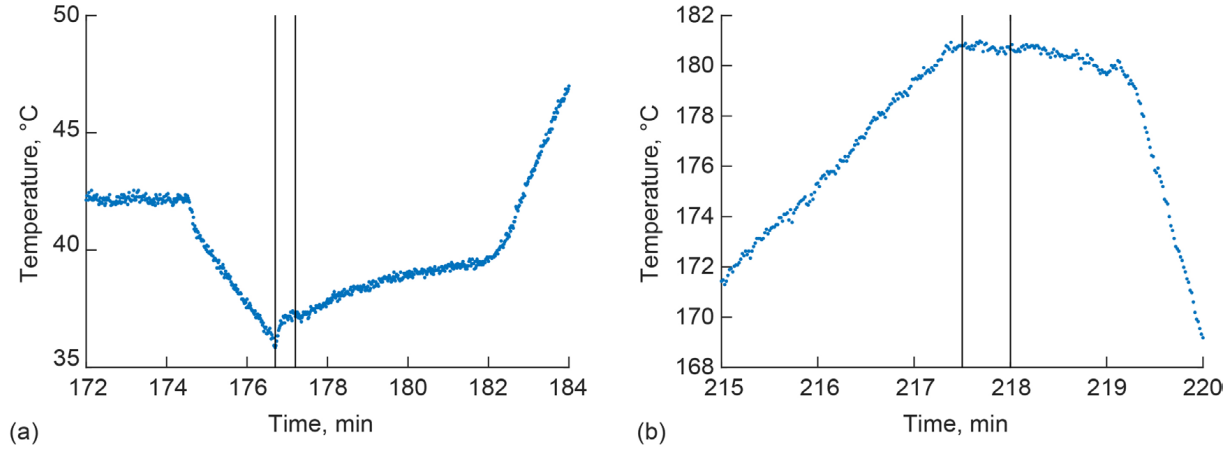

Figure 6.—Sample temperature versus hold time verification. Vertical bars indicate 30-s hold periods. (a) Lower cycle temperature. (b) Upper cycle temperature.

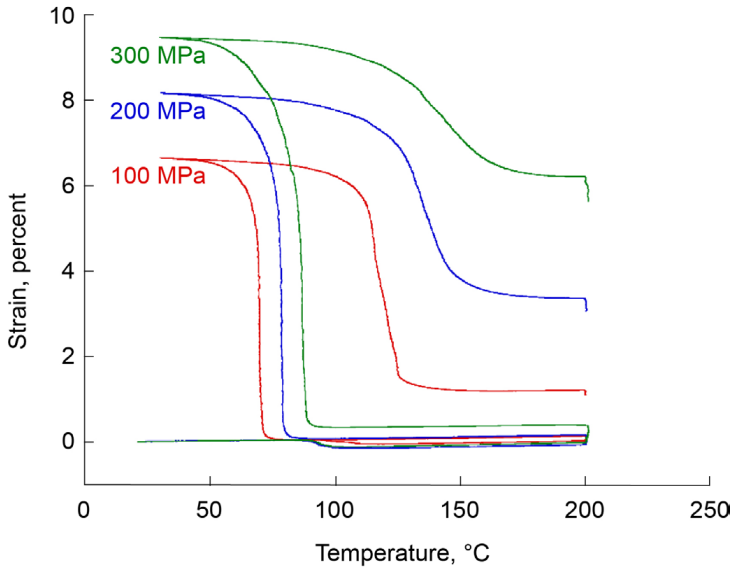

Figure 7.—Strain-temperature responses at different applied stresses.

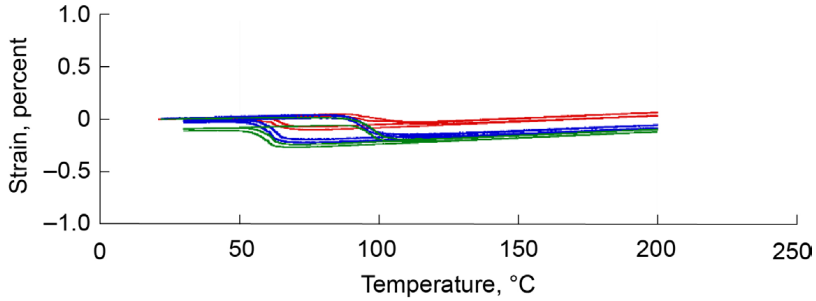

Figure 8.—Example normalization test for three different runs while holding stress at ~0 MPa.

4.3 Ruggedness Test Results

In addition to the half-normal plots, data were also presented in two other formats to observe trends and other potentially useful correlations. Each result variable related to this standard (23 in total, Figure 9 to Figure 31) was plotted as a function of run number including both replicates, and as a function of the low- and high-level settings corresponding to each factor listed in Table I.

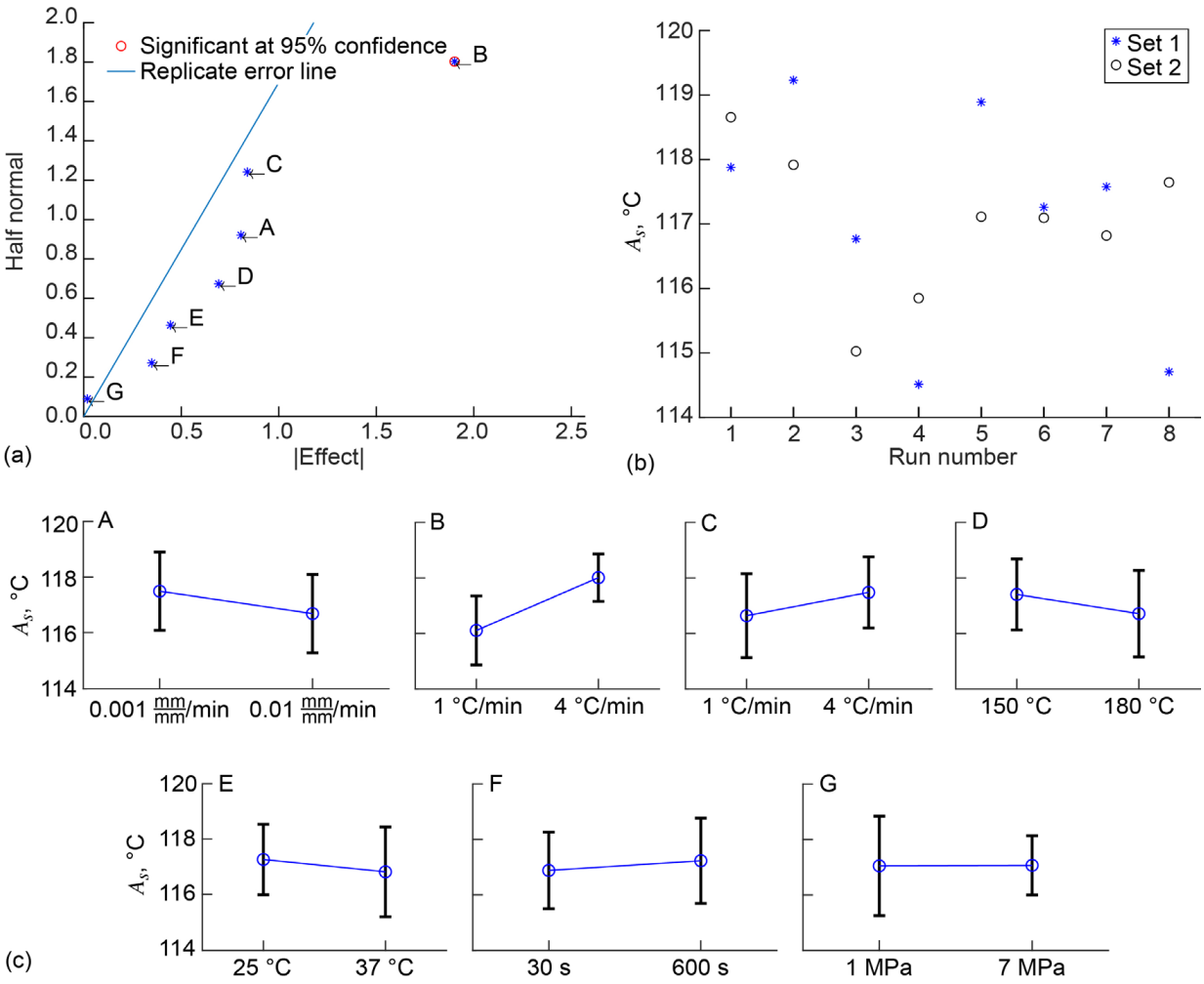

Figure 9.—Data, function of run number, and mean and standard deviation (STDEV) as a function of low- and high-level settings for austenite start, A_s. (a) Half-normal plot. (b) Function of run number for two replicates. (c) Mean and STDEV for A, strain rate; B, cooling rate; C, heating rate; D, upper cycle temperature (*UCT*); E, lower cycle temperature (*LCT*); F, hold time; and G, minimum load.

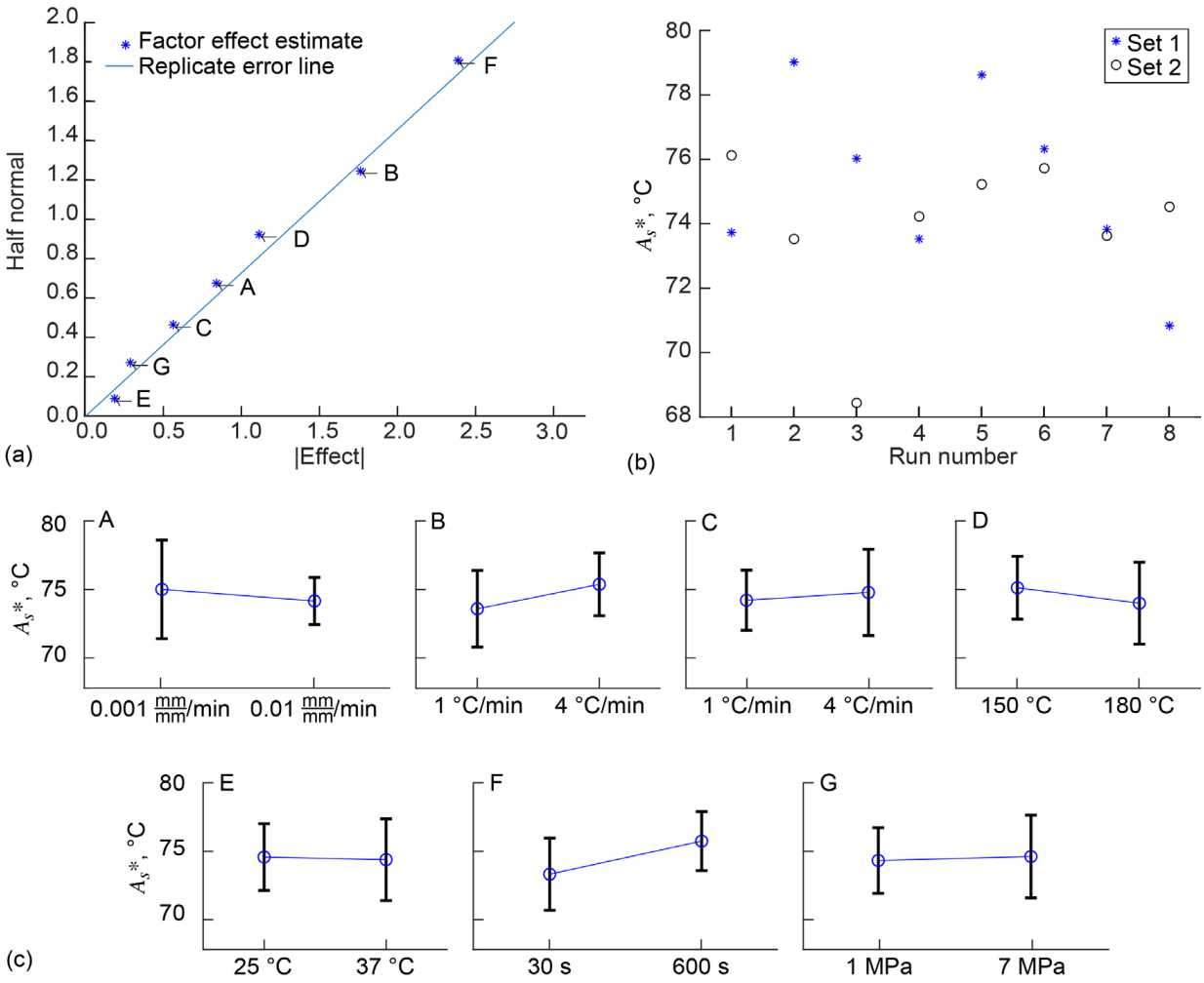

Figure 10.—Data, function of run number, and mean and standard deviation (STDEV) as a function of low- and high-level settings for austenite start tangent line and data intersect, A_s*. (a) Half-normal plot. (b) Function of run number for two replicates. (c) Mean and STDEV for A, strain rate; B, cooling rate; C, heating rate; D, upper cycle temperature (*UCT*); E, lower cycle temperature (*LCT*); F, hold time; and G, minimum load.

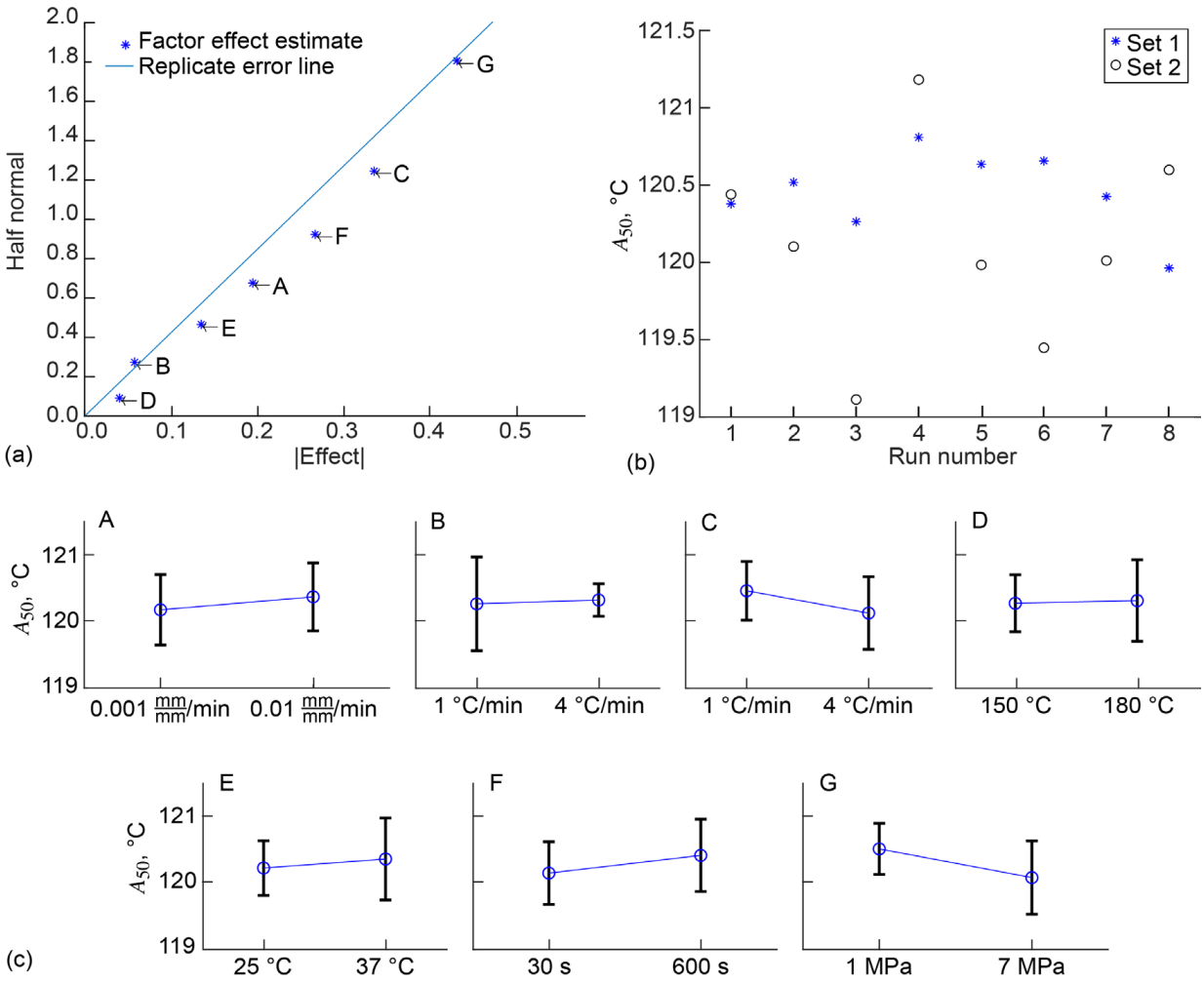

Figure 11.—Data, function of run number, and mean and standard deviation (STDEV) as a function of low- and high-level settings for austenite 50 percent, A_{50}. (a) Half-normal plot. (b) Function of run number for two replicates. (c) Mean and STDEV for A, strain rate; B, cooling rate; C, heating rate; D, upper cycle temperature (*UCT*); E, lower cycle temperature (*LCT*); F, hold time; and G, minimum load.

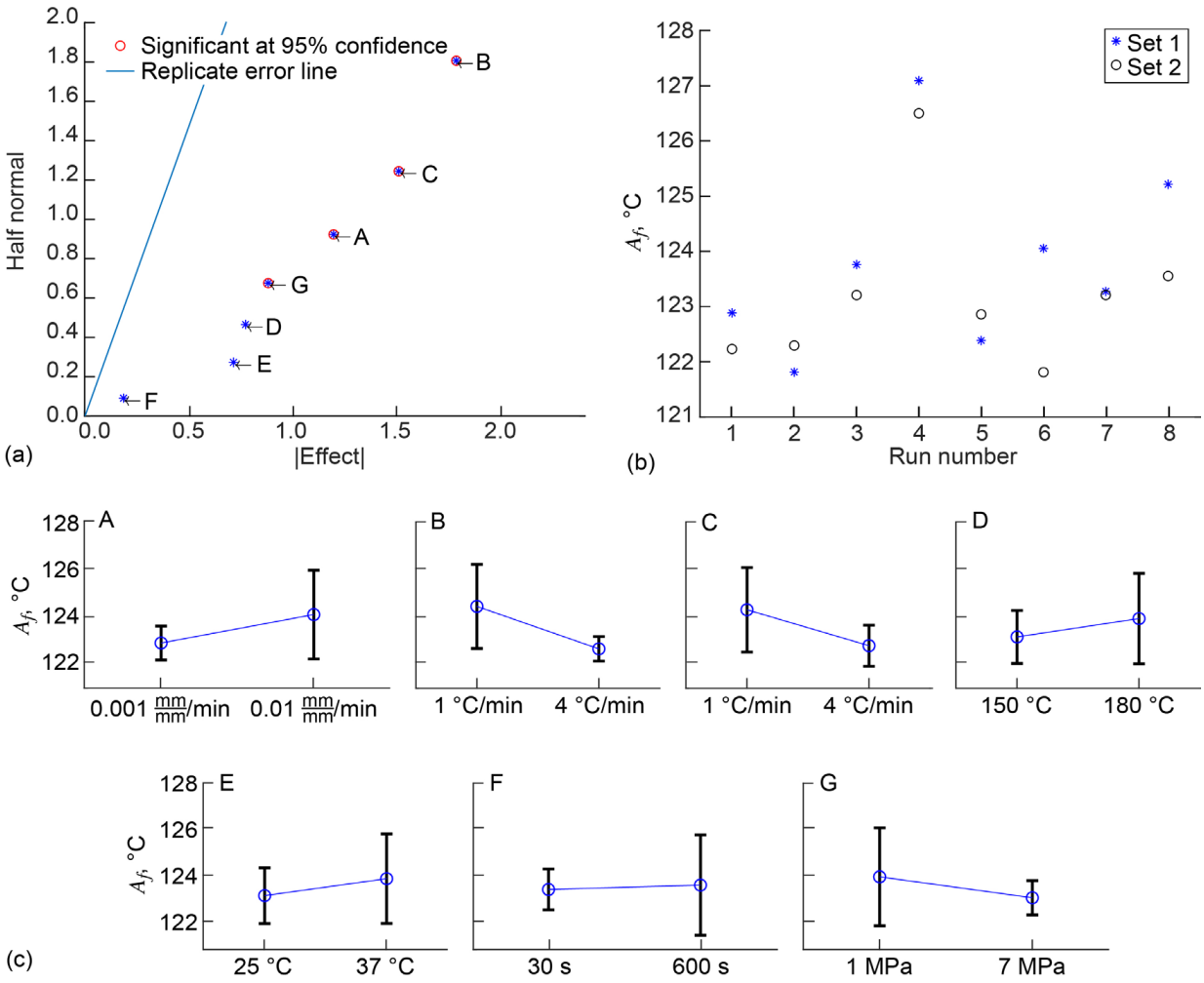

Figure 12.—Data, function of run number, and mean and standard deviation (STDEV) as a function of low- and high-level settings for austenite finish, A_f. (a) Half-normal plot. (b) Function of run number for two replicates. (c) Mean and STDEV for A, strain rate; B, cooling rate; C, heating rate; D, upper cycle temperature (*UCT*); E, lower cycle temperature (*LCT*); F, hold time; and G, minimum load.

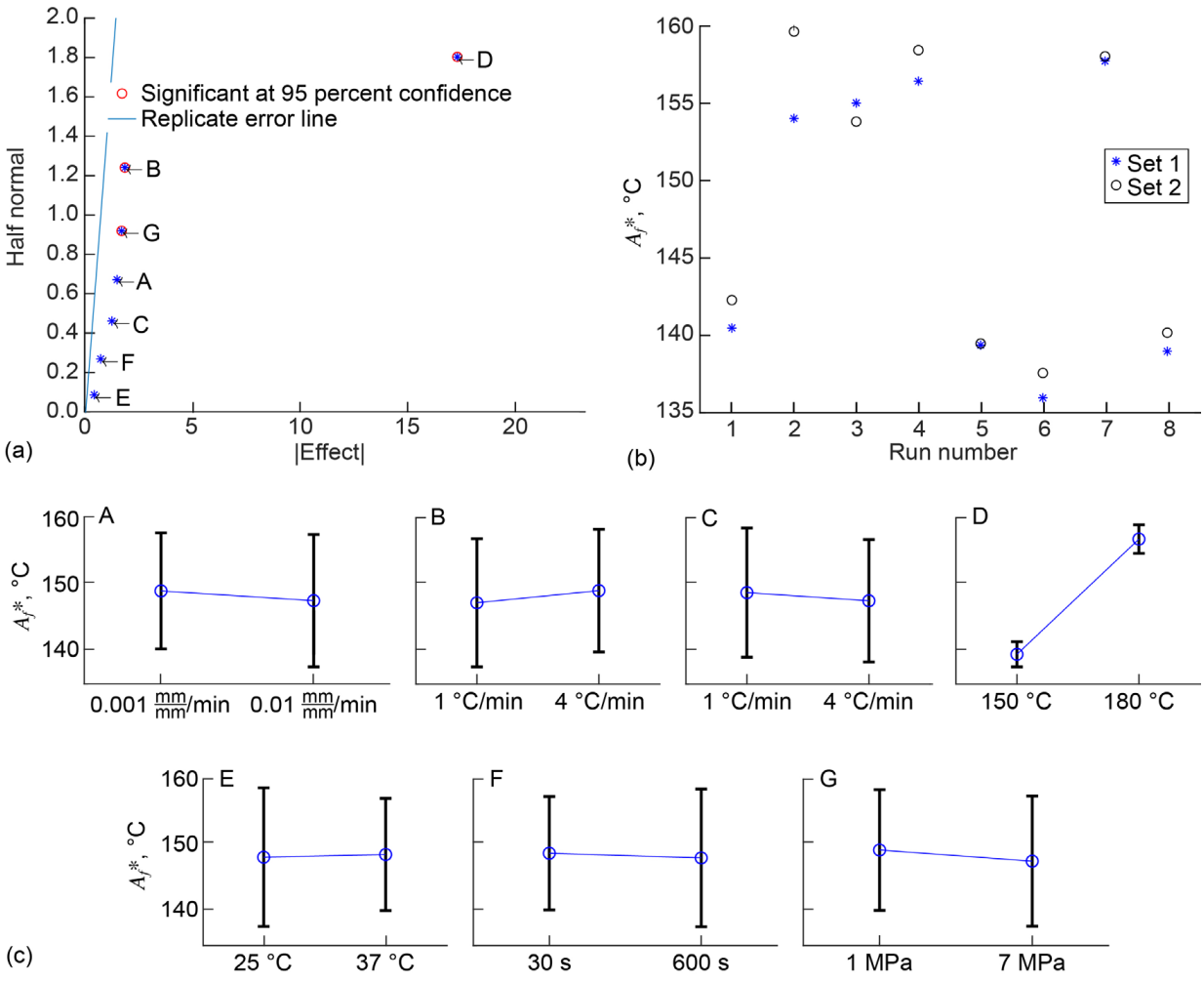

Figure 13.—Data, function of run number, and mean and standard deviation (STDEV) as a function of low- and high-level settings for austenite finish tangent line and data intersect, A_f*. (a) Half-normal plot. (b) Function of run number for two replicates. (c) Mean and standard deviation for A, strain rate; B, cooling rate; C, heating rate; D, upper cycle temperature (*UCT*); E, lower cycle temperature (*LCT*); F, hold time; and G, minimum load.

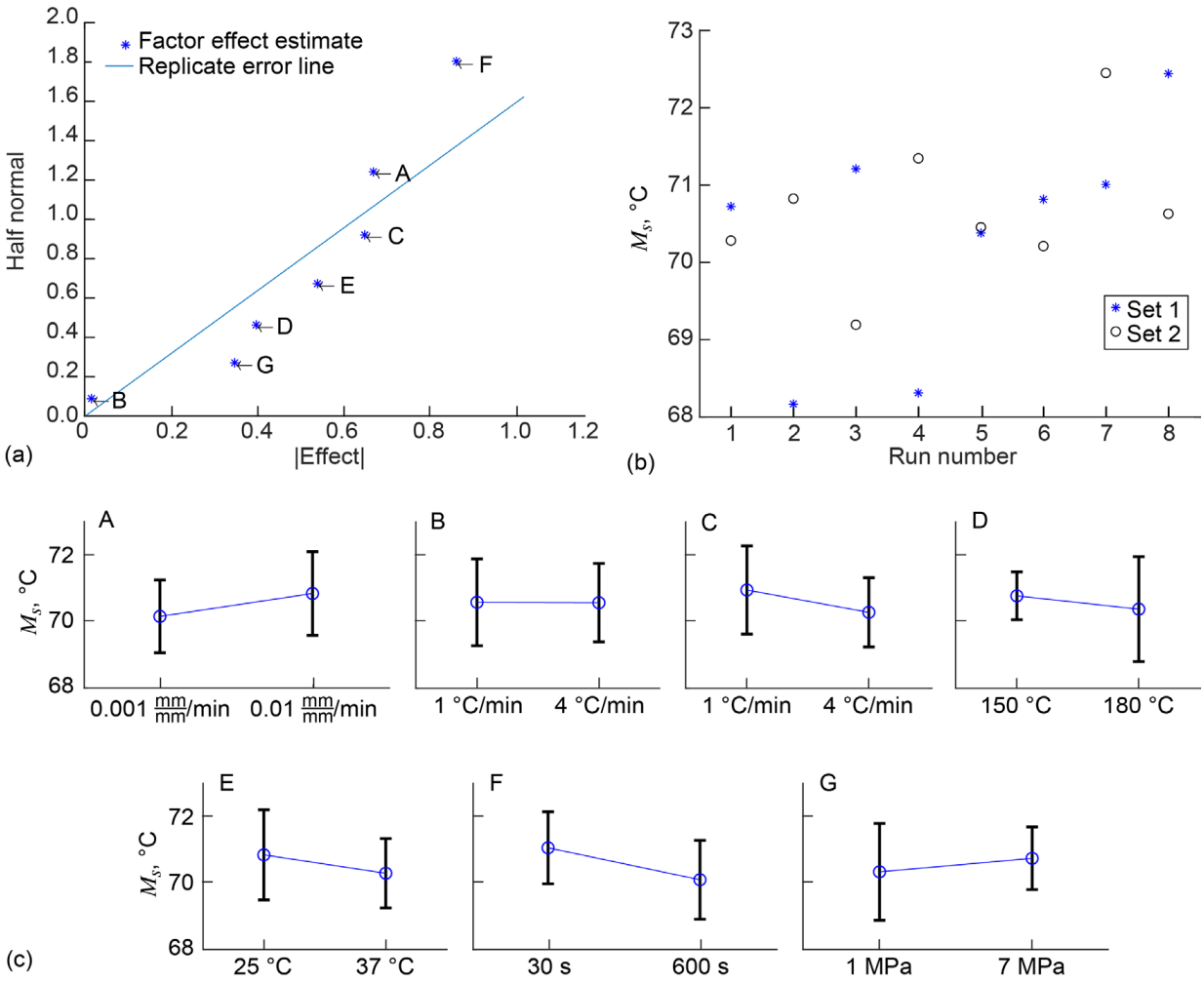

Figure 14.—Data, function of run number, and mean and standard deviation (STDEV) as a function of low- and high-level settings for martensite start, M_s. (a) Half-normal plot. (b) Function of run number for two replicates. (c) Mean and STDEV for A, strain rate; B, cooling rate; C, heating rate; D, upper cycle temperature (*UCT*); E, lower cycle temperature (*LCT*); F, hold time; and G, minimum load.

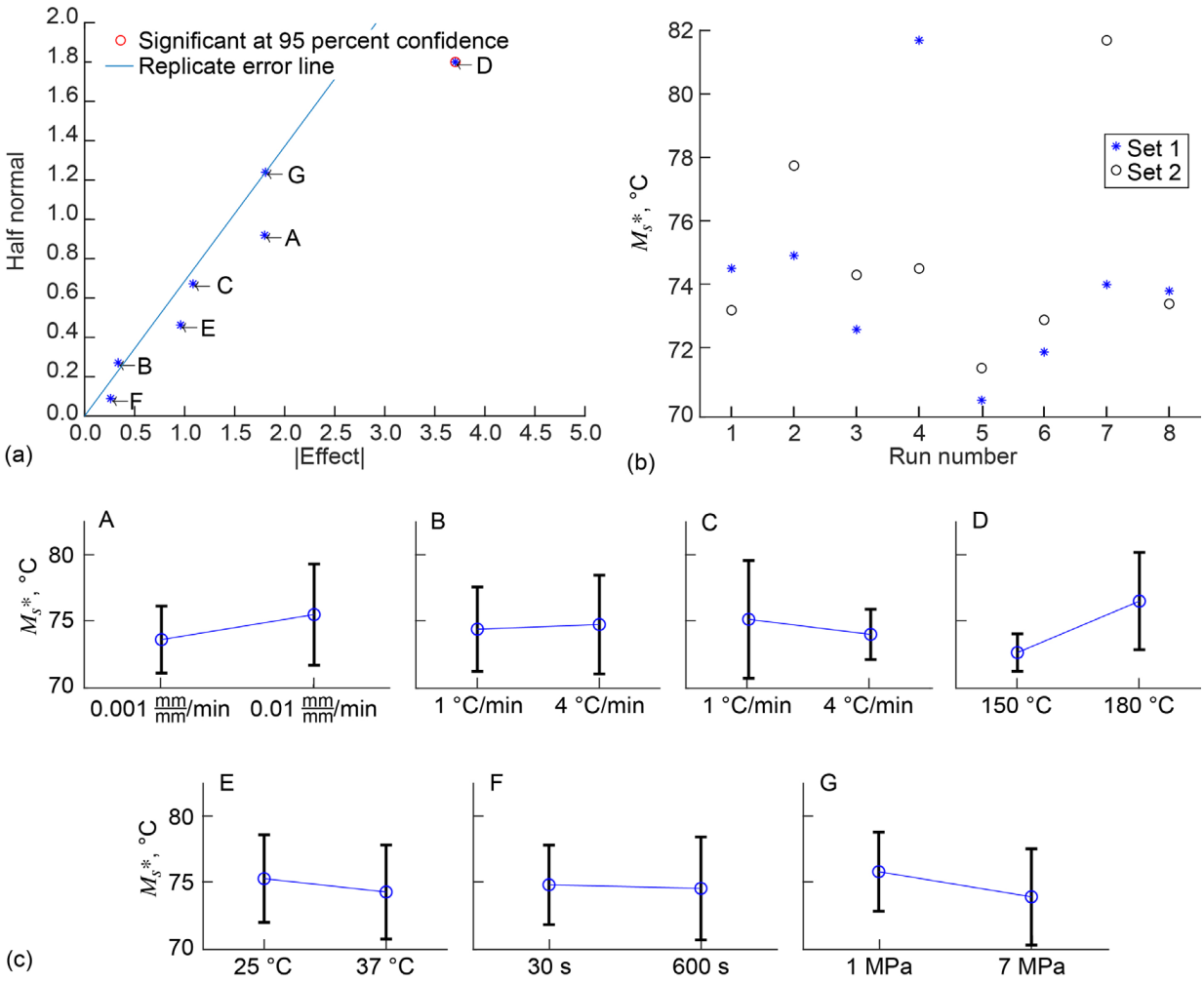

Figure 15.—Data, function of run number, and mean and standard deviation (STDEV) as a function of low- and high-level settings for martensite start tangent line and data intersect, M_s*. (a) Half-normal plot. (b) Function of run number for two replicates. (c) Mean and STDEV for A, strain rate; B, cooling rate; C, heating rate; D, upper cycle temperature (*UCT*); E, lower cycle temperature (*LCT*); F, hold time; and G, minimum load.

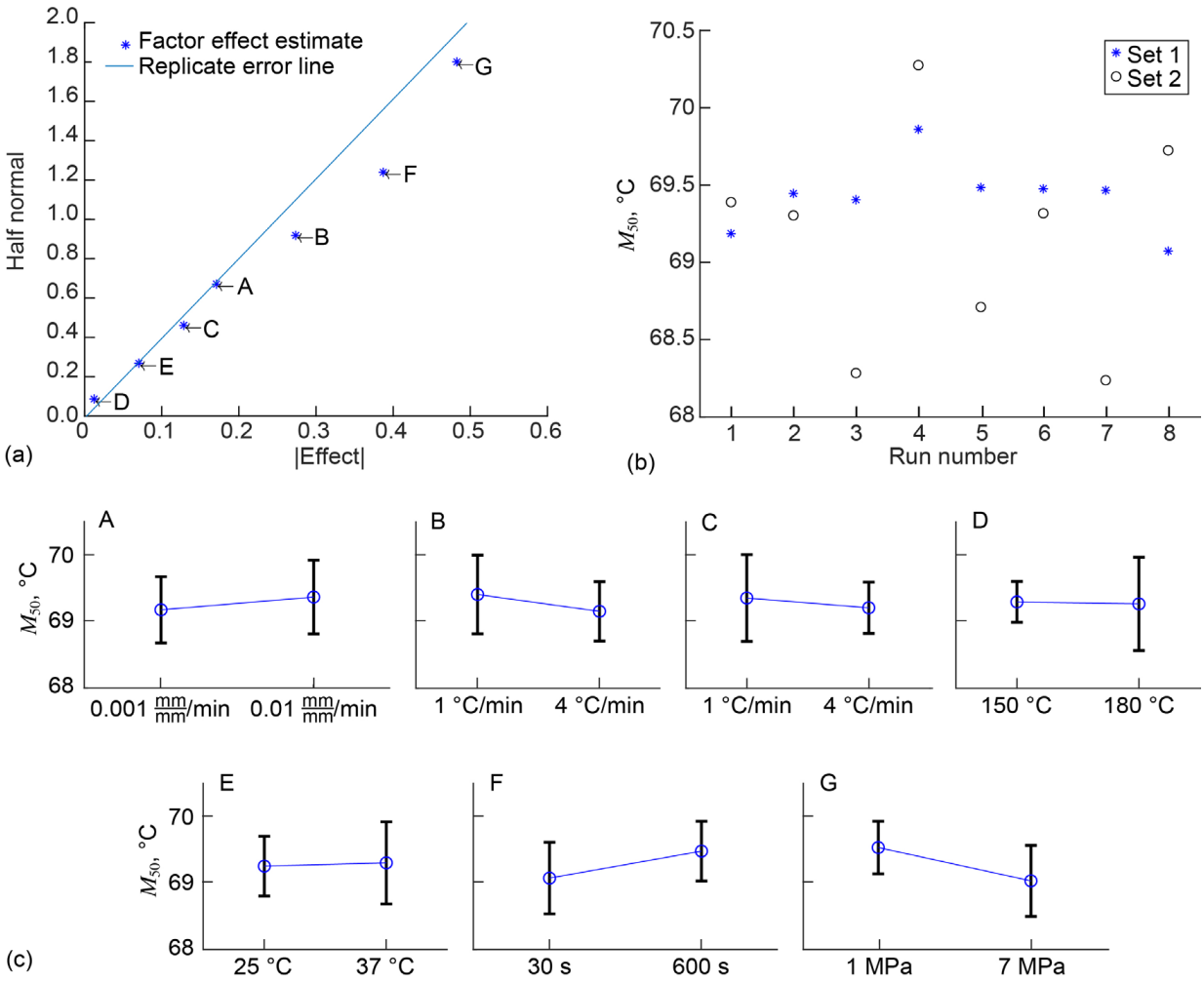

Figure 16.—Data, function of run number, and mean and standard deviation (STDEV) as a function of low- and high-level settings for martensite 50 percent, M_{50}. (a) Half-normal plot. (b) Function of run number for two replicates. (c) Mean and STDEV for A, strain rate; B, cooling rate; C, heating rate; D, upper cycle temperature (*UCT*); E, lower cycle temperature (*LCT*); F, hold time; and G, minimum load.

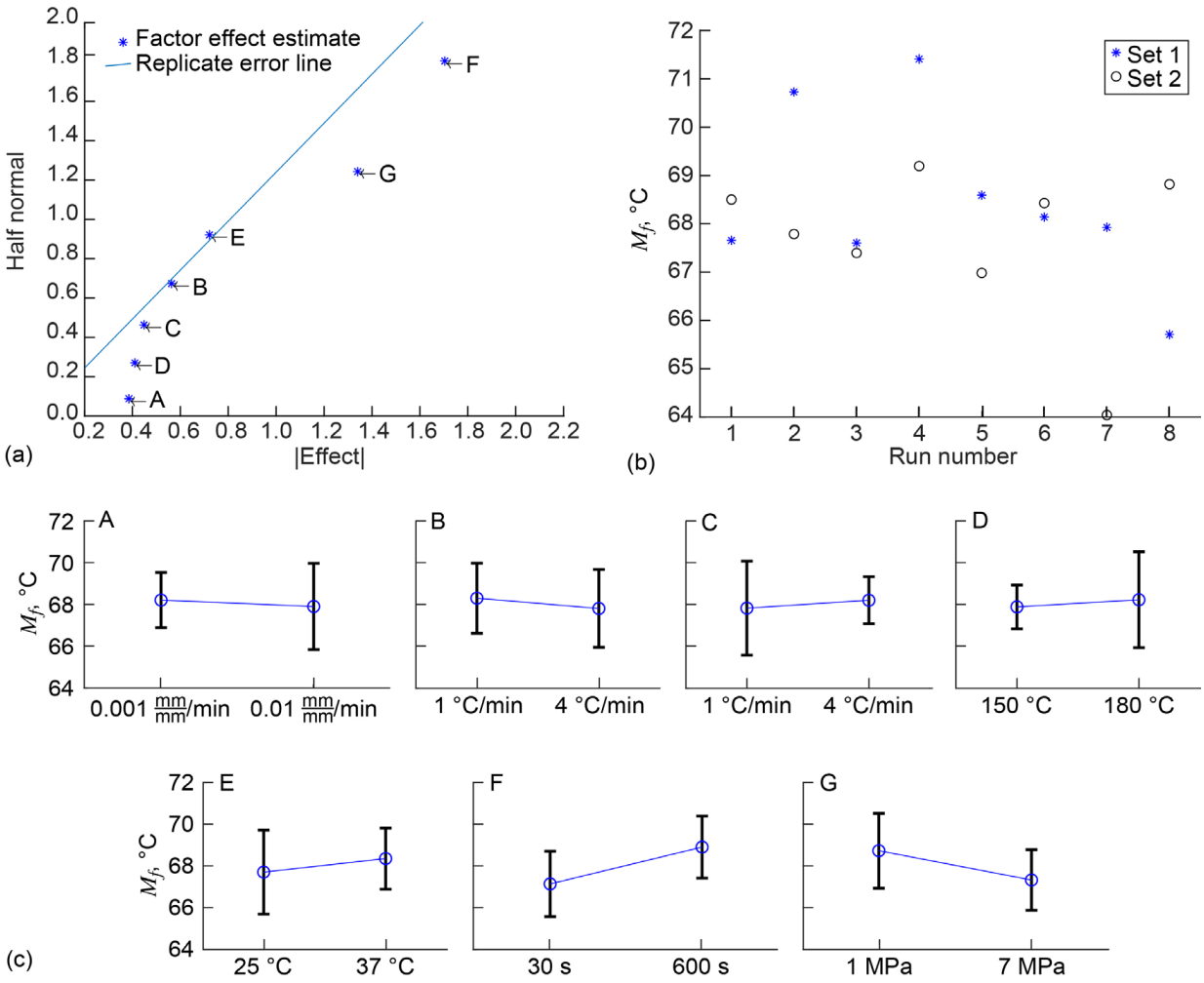

Figure 17.—Data, function of run number, and mean and standard deviation (STDEV) as a function of low- and high-level settings for martensite finish, M_f. (a) Half-normal plot. (b) Function of run number for two replicates. (c) Mean and STDEV for A, strain rate; B, cooling rate; C, heating rate; D, upper cycle temperature (*UCT*); E, lower cycle temperature (*LCT*); F, hold time; and G, minimum load.

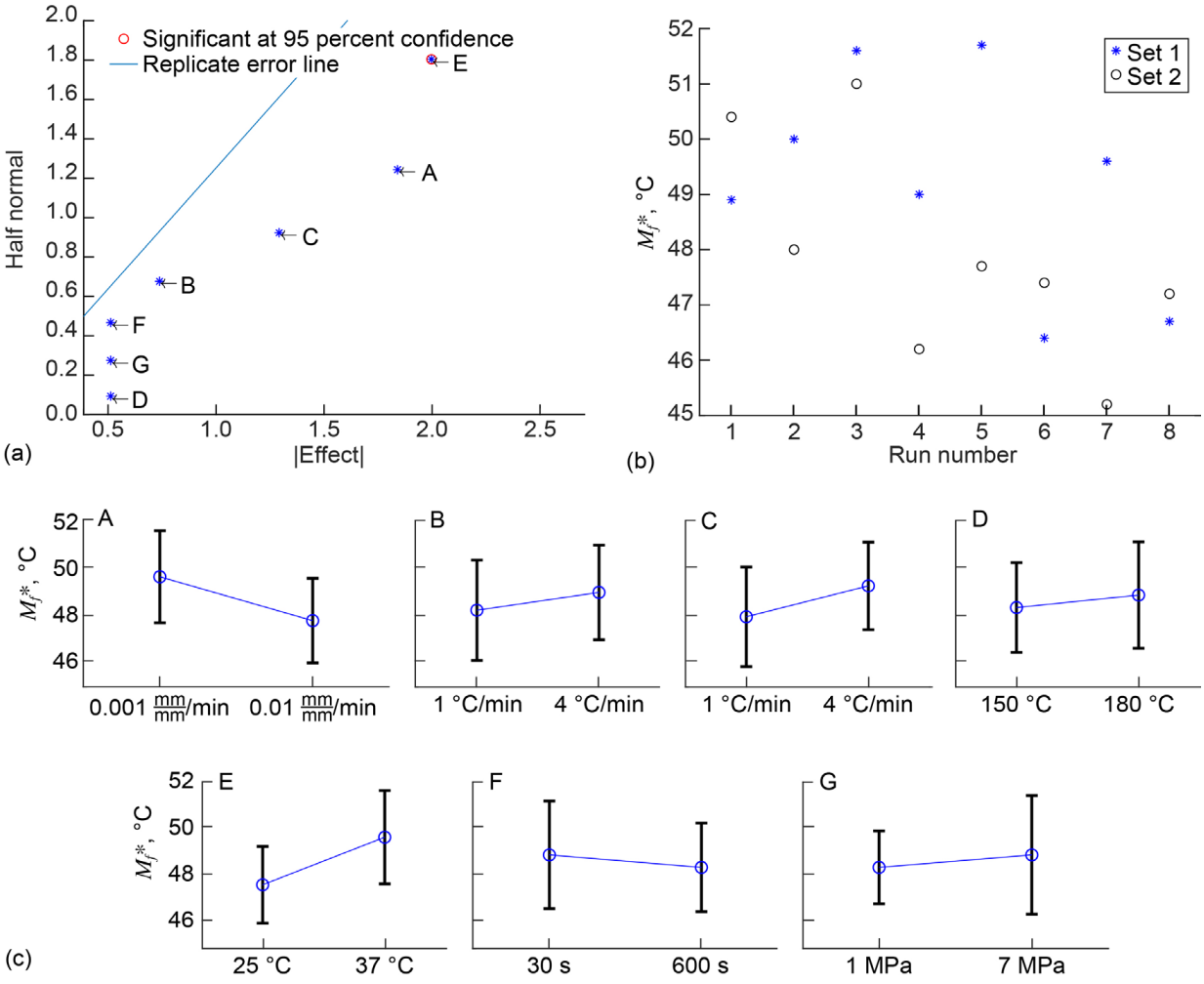

Figure 18.—Data, function of run number, and mean and standard deviation (STDEV) as a function of low- and high-level settings for martensite finish tangent line and data intersect, M_f*. (a) Half-normal plot. (b) Function of run number for two replicates. (c) Mean and STDEV for A, strain rate; B, cooling rate; C, heating rate; D, upper cycle temperature (UCT); E, lower cycle temperature (LCT); F, hold time; and G, minimum load.

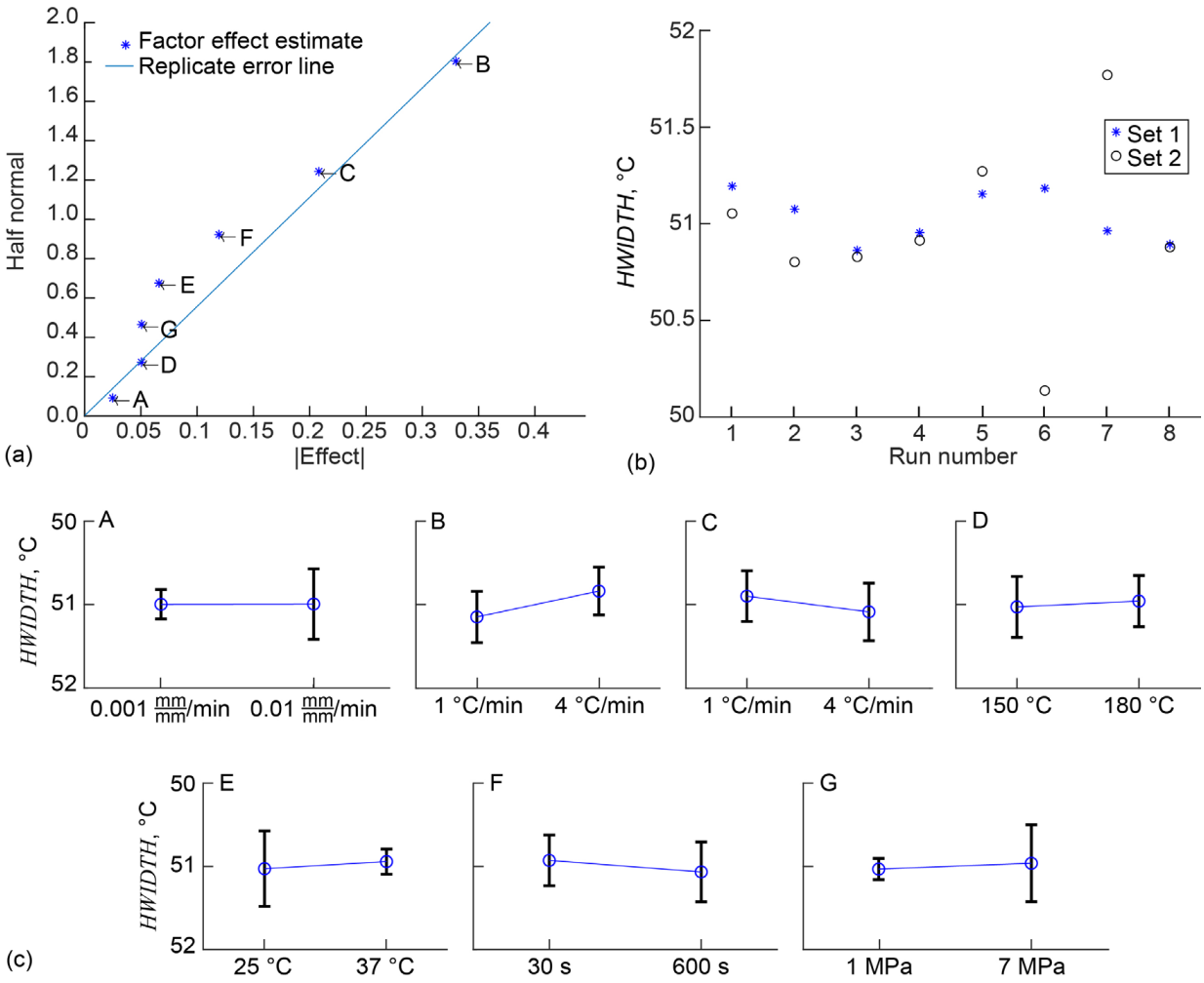

Figure 19.—Data, function of run number, and mean and standard deviation (STDEV) as a function of low- and high-level settings for hysteresis width, *HWIDTH*. (a) Half-normal plot. (b) Function of run number for two replicates. (c) Mean and STDEV for A, strain rate; B, cooling rate; C, heating rate; D, upper cycle temperature (*UCT*); E, lower cycle temperature (*LCT*); F, hold time; and G, minimum load.

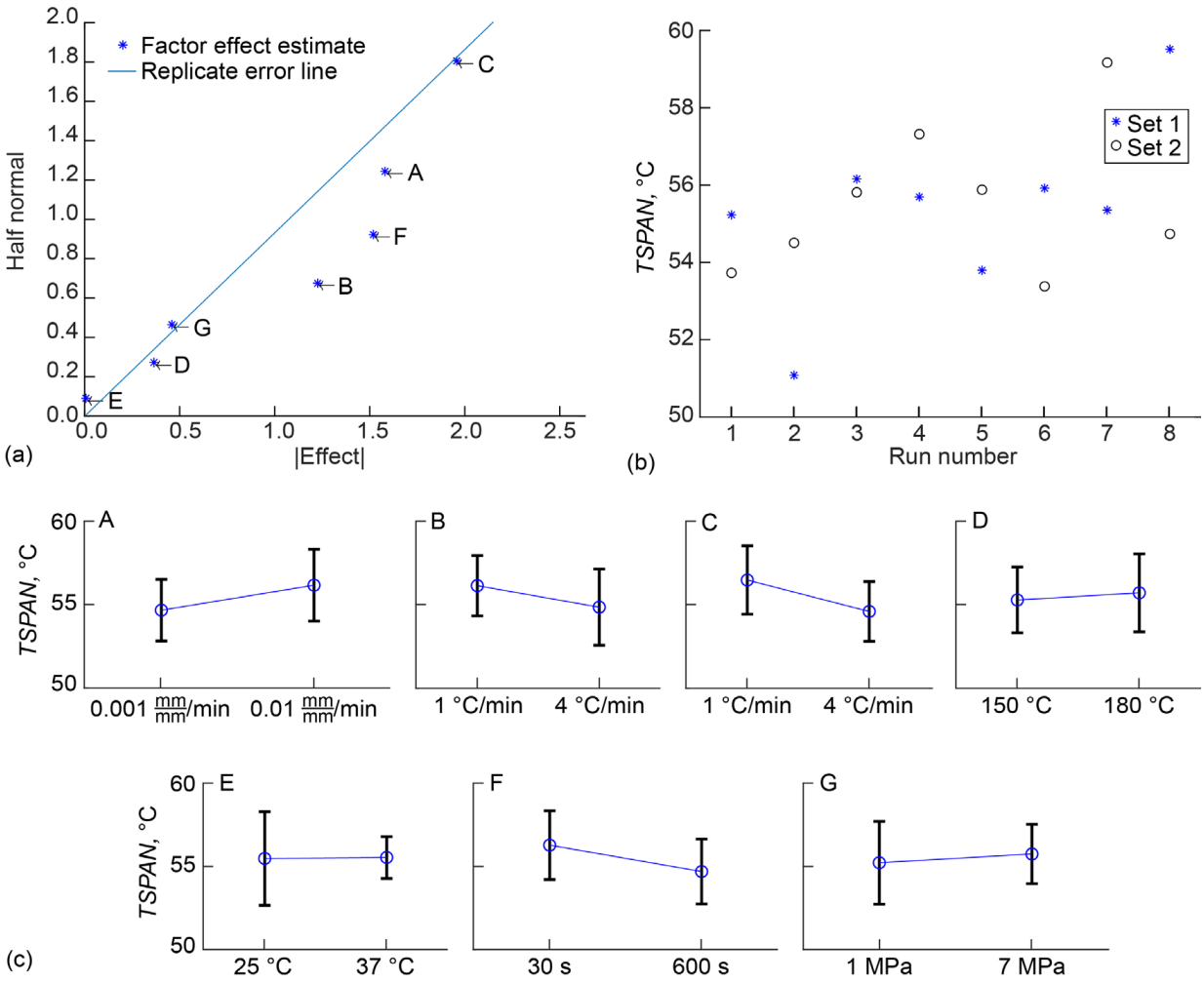

Figure 20.—Data, function of run number, and mean and standard deviation (STDEV) as a function of low- and high-level settings for thermal transformation span, *TSPAN*. (a) Half-normal plot. (b) Function of run number for two replicates. (c) Mean and STDEV for A, strain rate; B, cooling rate; C, heating rate; D, upper cycle temperature (*UCT*); E, lower cycle temperature (*LCT*); F, hold time; and G, minimum load.

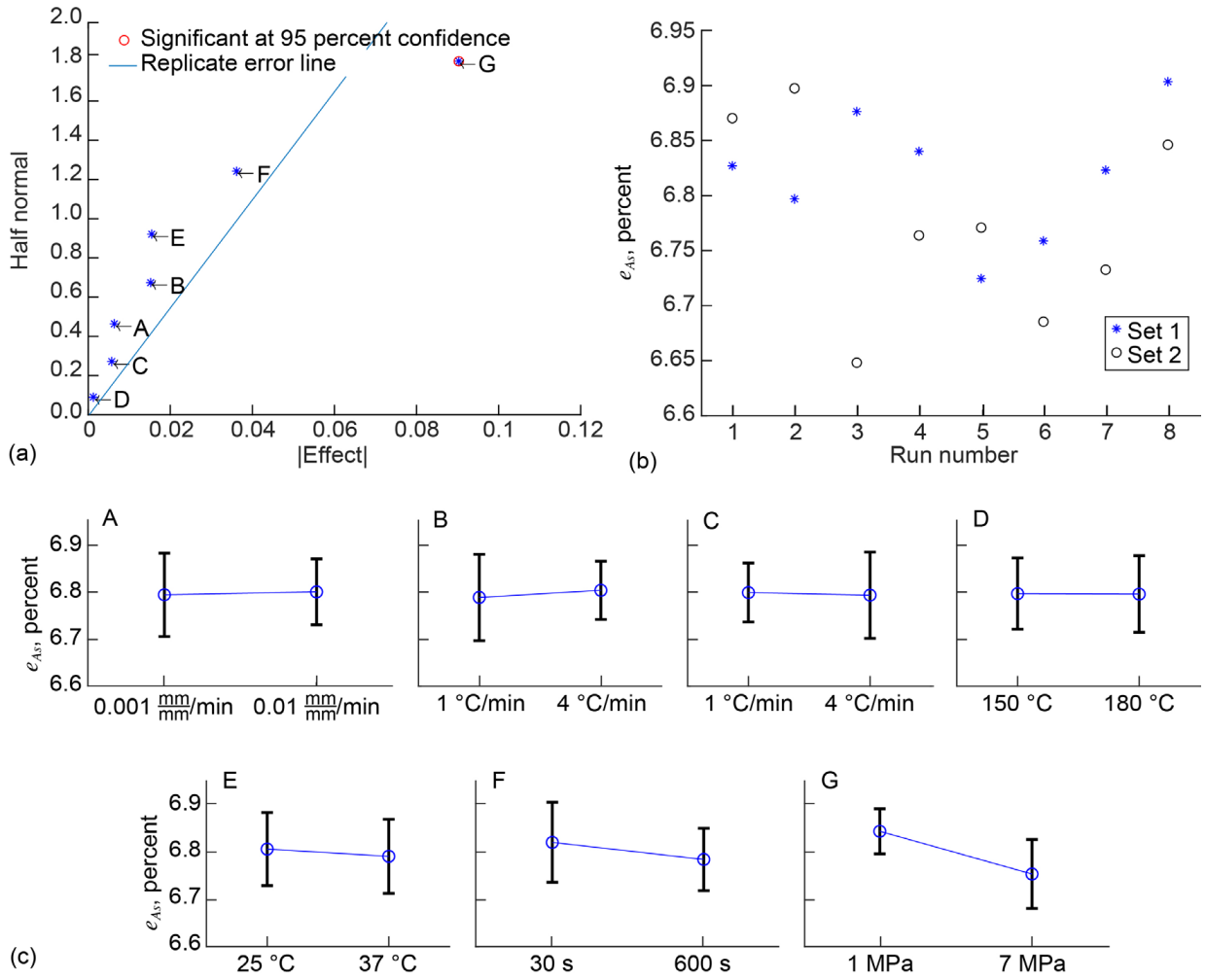

Figure 21.—Data, function of run number, and mean and standard deviation (STDEV) as a function of low- and high-level settings for strain at austenite start temperature (fit line intersection point), e_{As}. (a) Half-normal plot. (b) Function of run number for two replicates. (c) Mean and STDEV for A, strain rate; B, cooling rate; C, heating rate; D, upper cycle temperature (*UCT*); E, lower cycle temperature (*LCT*); F, hold time; and G, minimum load.

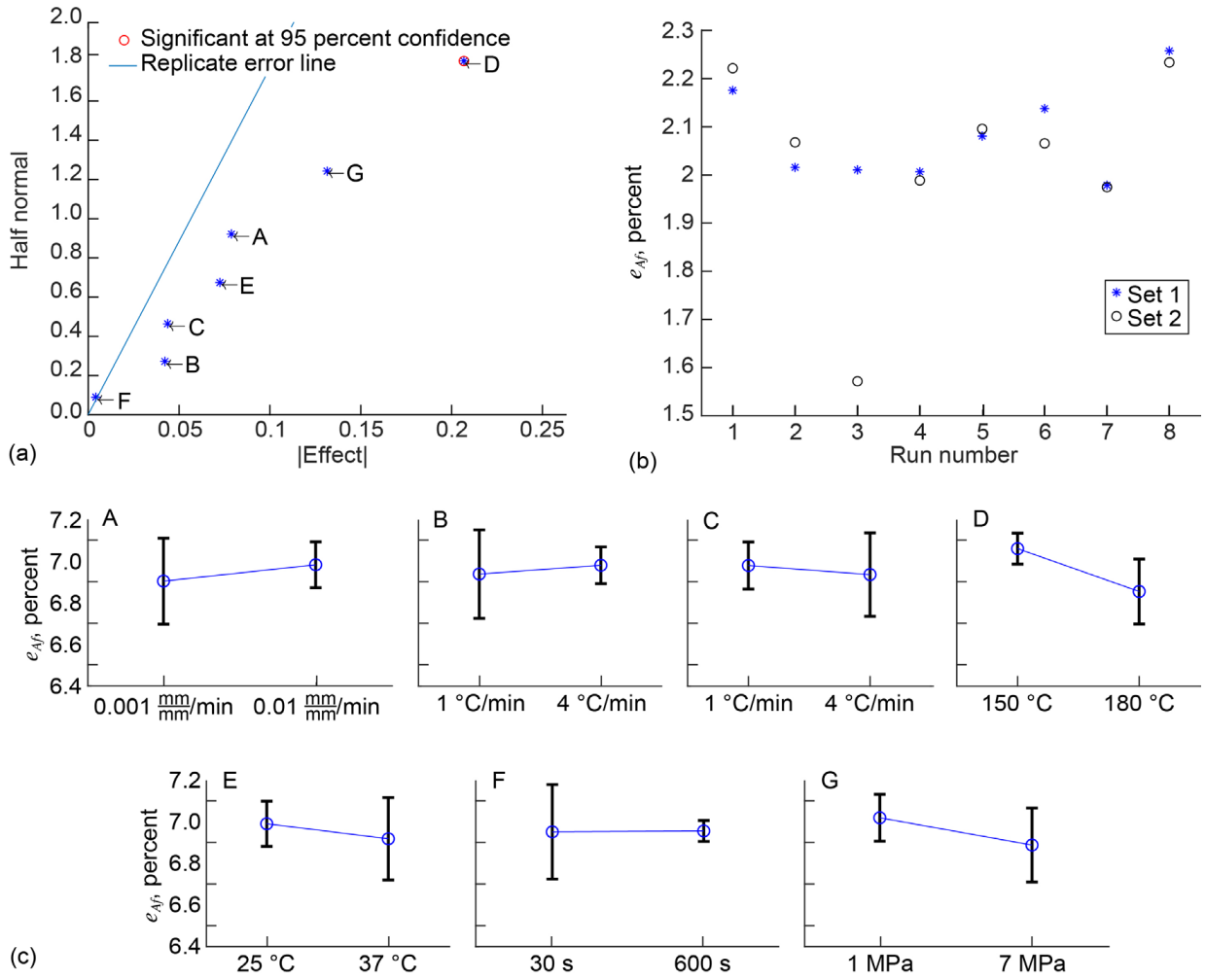

Figure 22.—Data, function of run number, and mean and standard deviation (STDEV) as a function of low- and high-level settings for strain at austenite finish temperature (fit line intersection point), e_{Af}. (a) Half-normal plot. (b) Function of run number for two replicates. (c) Mean and STDEV for A, strain rate; B, cooling rate; C, heating rate; D, upper cycle temperature (*UCT*); E, lower cycle temperature (*LCT*); F, hold time; and G, minimum load.

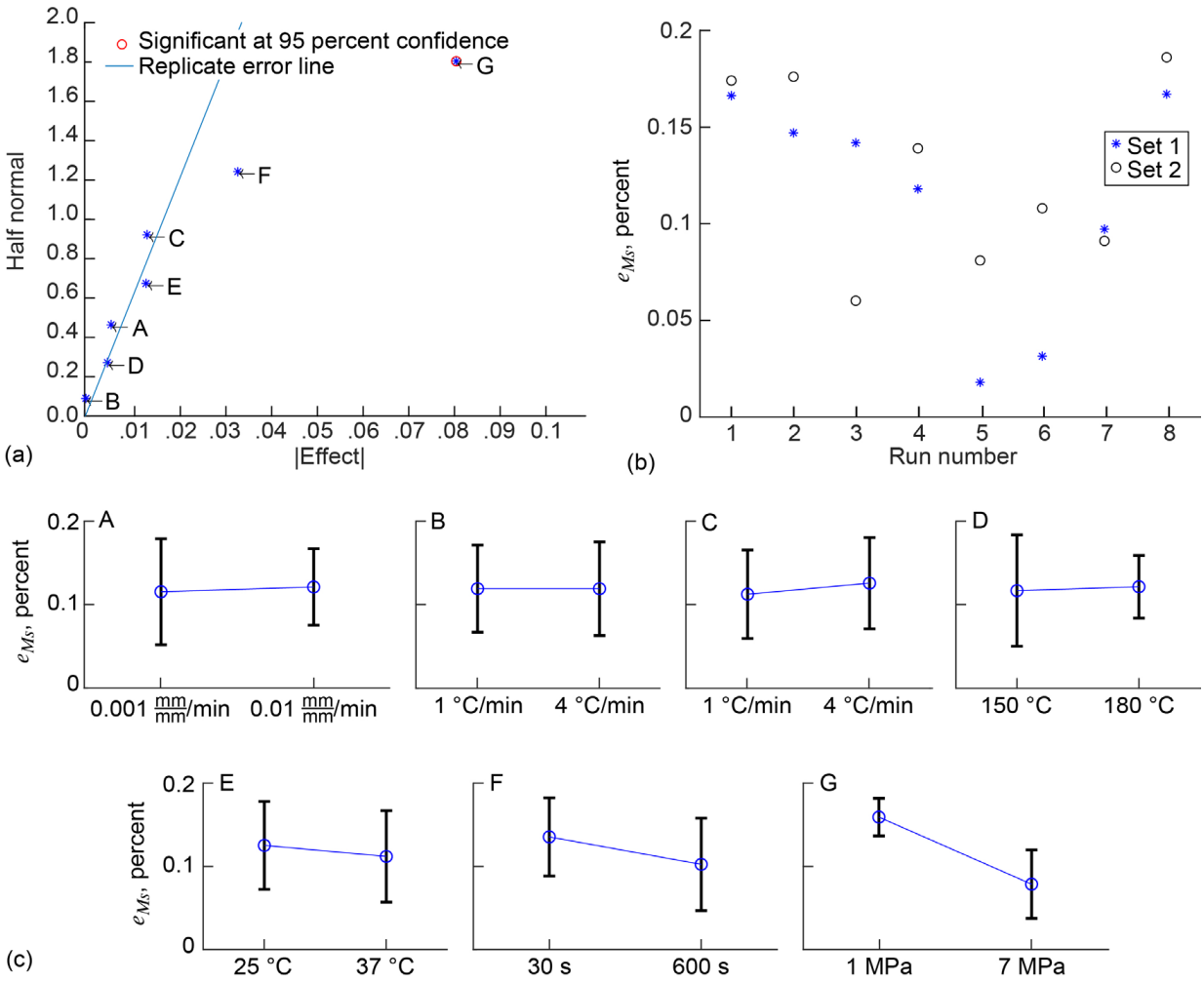

Figure 23.—Data, function of run number, and mean and standard deviation (STDEV) as a function of low- and high-level settings for strain at martensite start temperature (fit line intersection point), e_{Ms}. (a) Half-normal plot. (b) Function of run number for two replicates. (c) Mean and STDEV for A, strain rate; B, cooling rate; C, heating rate; D, upper cycle temperature (*UCT*); E, lower cycle temperature (*LCT*); F, hold time; and G, minimum load.

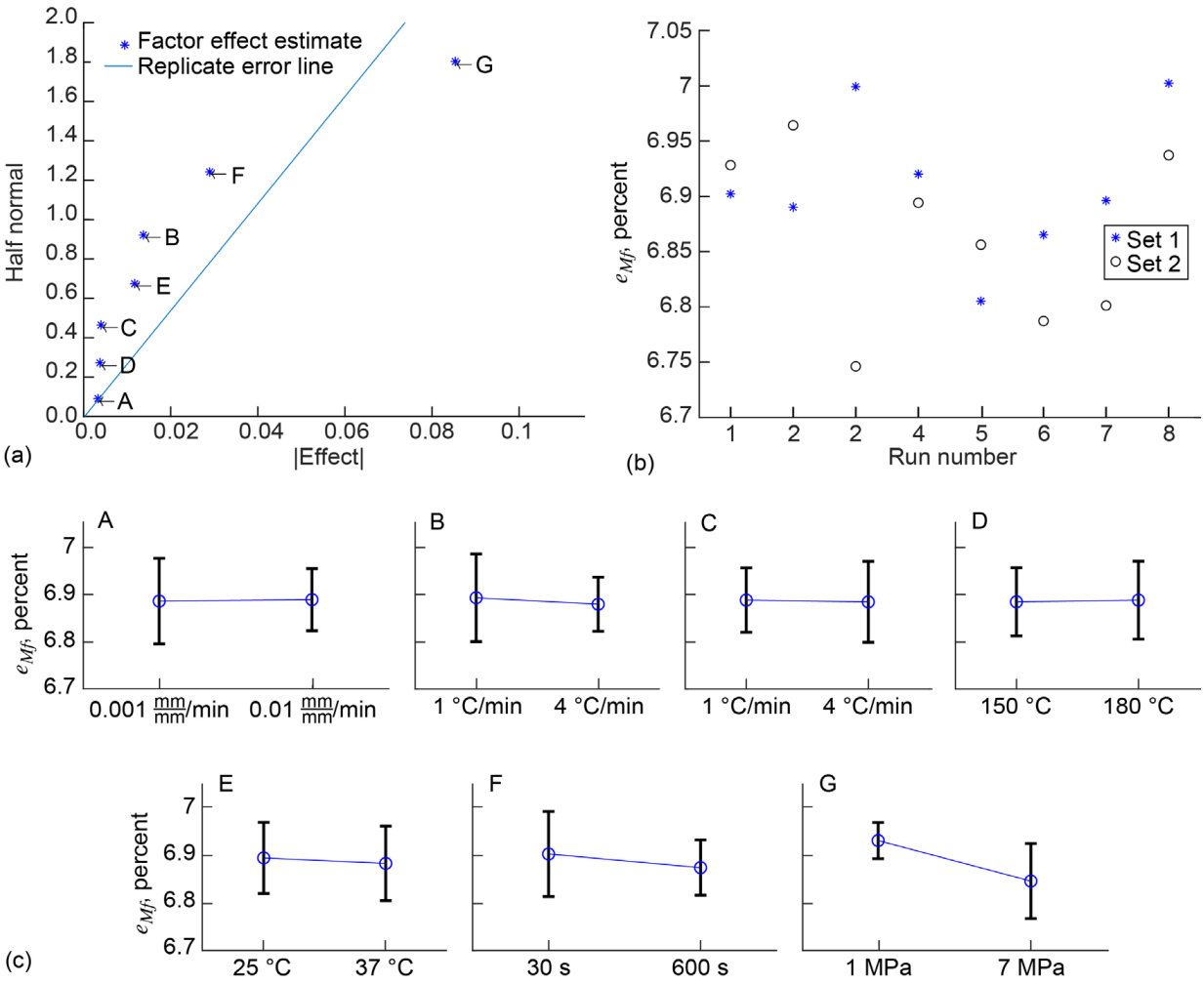

Figure 24.—Data, function of run number, and mean and standard deviation (STDEV) as a function of low- and high-level settings for strain at martensite finish temperature (fit line intersection point), e_{Mf}. (a) Half-normal plot. (b) Function of run number for two replicates. (c) Mean and STDEV for A, strain rate; B, cooling rate; C, heating rate; D, upper cycle temperature (UCT); E, lower cycle temperature (LCT); F, hold time; and G, minimum load.

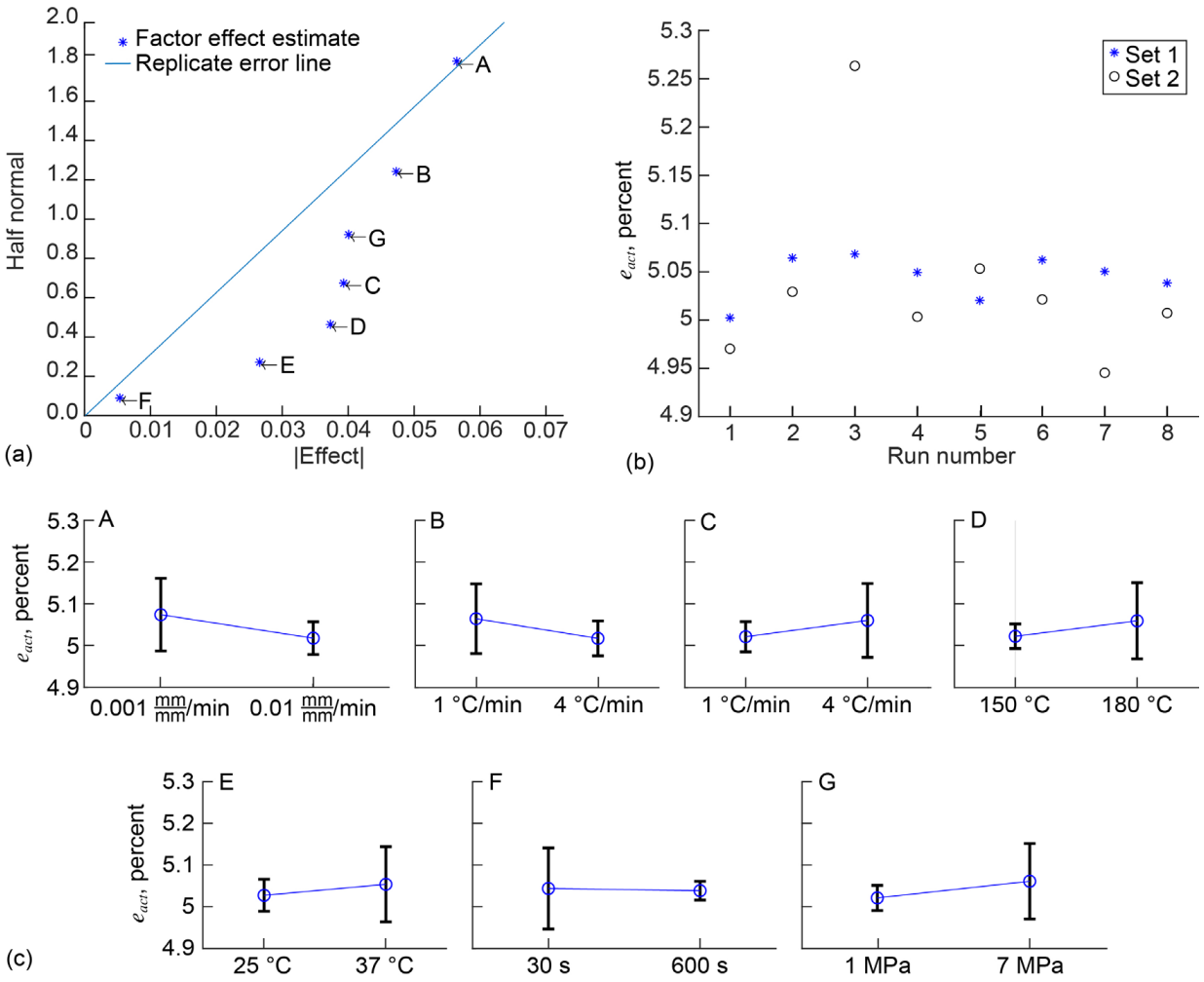

Figure 25.—Data, function of run number, and mean and standard deviation (STDEV) as a function of low- and high-level settings for actuation strain, e_{act}. (a) Half-normal plot. (b) Function of run number for two replicates. (c) Mean and STDEV for A, strain rate; B, cooling rate; C, heating rate; D, upper cycle temperature (*UCT*); E, lower cycle temperature (*LCT*); F, hold time; and G, minimum load.

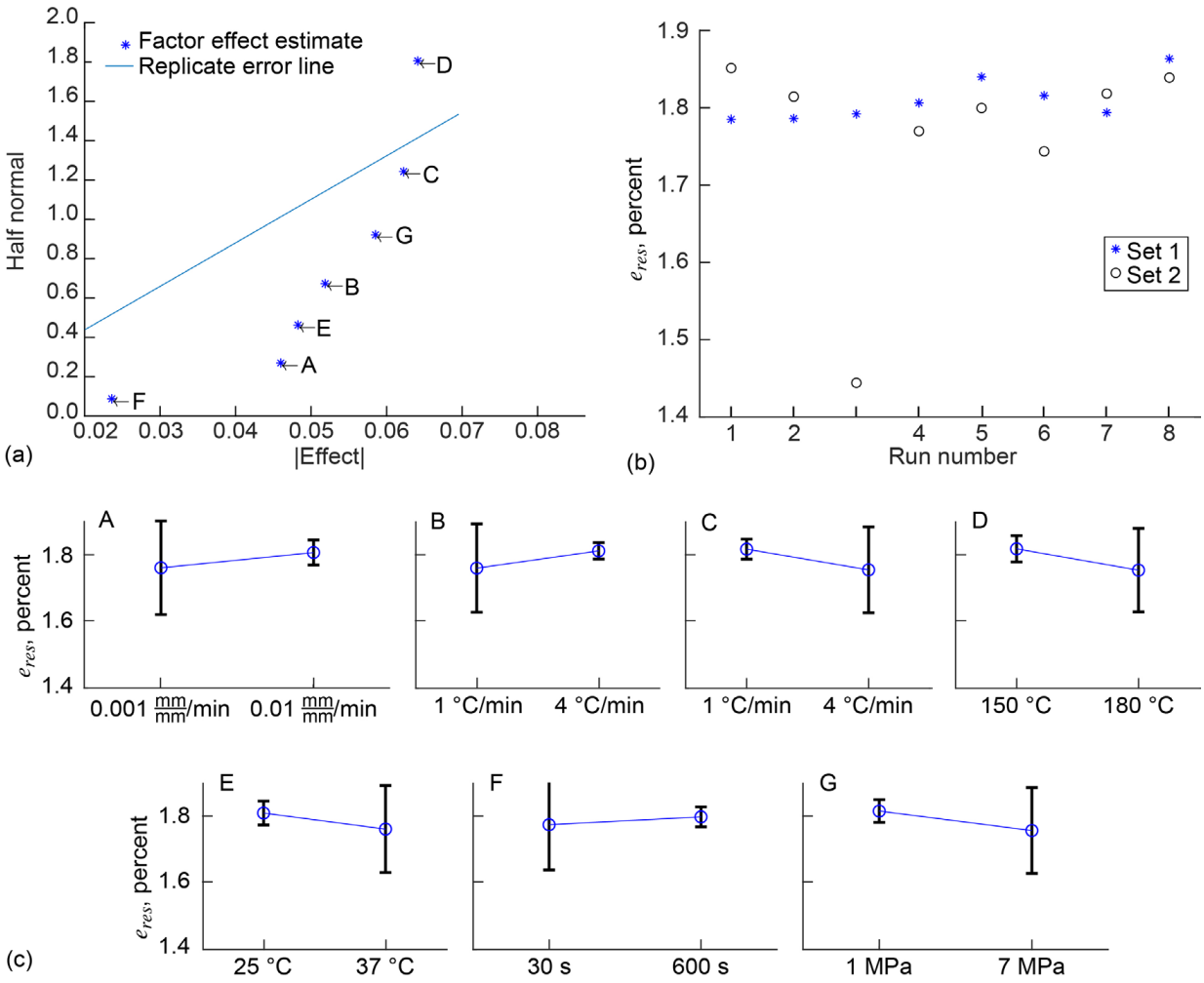

Figure 26.—Data, function of run number, and mean and standard deviation (STDEV) as a function of low- and high-level settings for residual strain, e_{res}. (a) Half-normal plot. (b) Function of run number for two replicates. (c) Mean and STDEV for A, strain rate; B, cooling rate; C, heating rate; D, upper cycle temperature (*UCT*); E, lower cycle temperature (*LCT*); F, hold time; and G, minimum load.

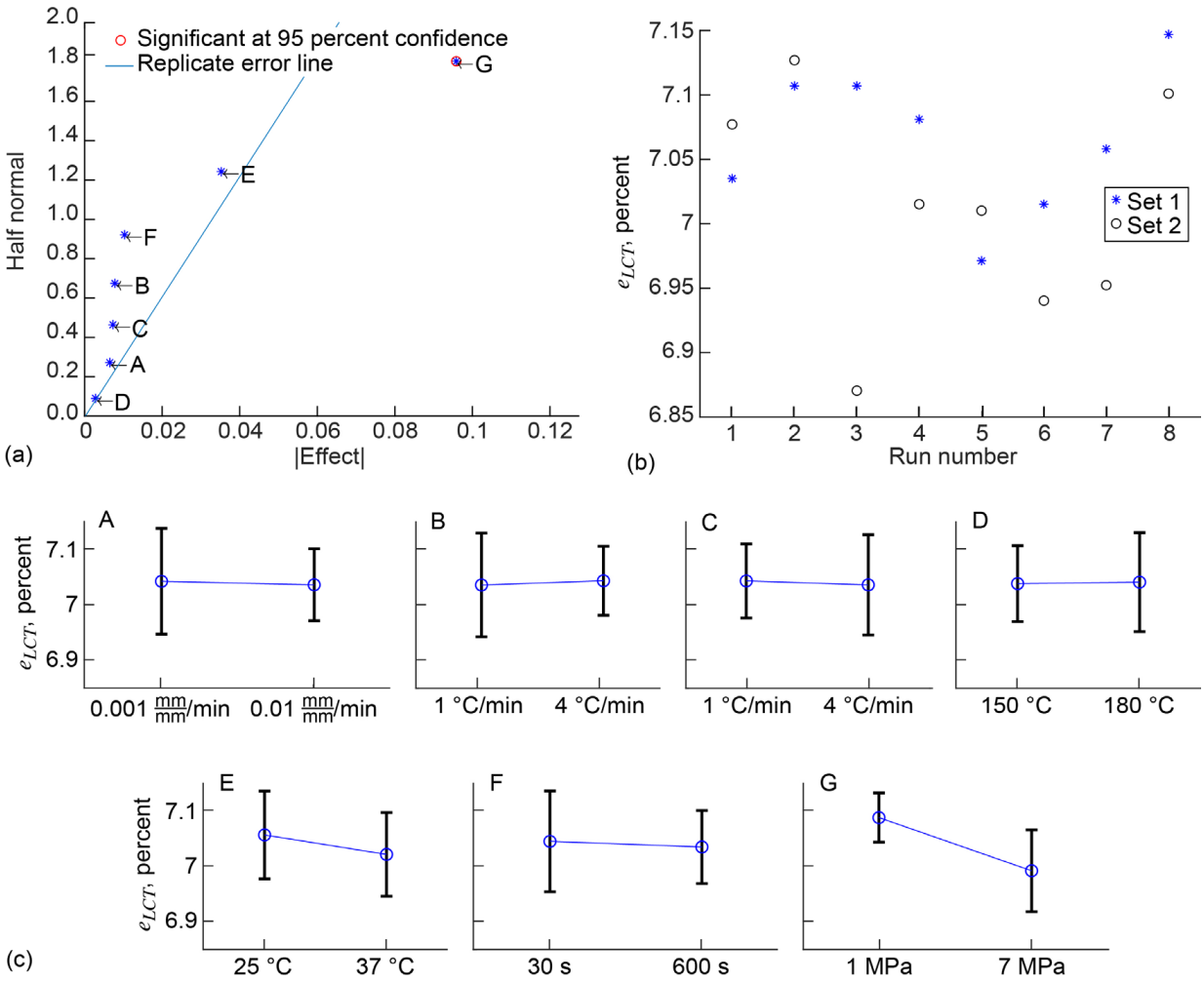

Figure 27.—Data, function of run number, and mean and standard deviation (STDEV) as a function of low- and high-level settings for strain at lower cycle temperature (after cooling under load), e_{LCT}. (a) Half-normal plot. (b) Function of run number for two replicates. (c) Mean and STDEV for A, strain rate; B, cooling rate; C, heating rate; D, upper cycle temperature (*UCT*); E, lower cycle temperature (*LCT*); F, hold time; and G, minimum load.

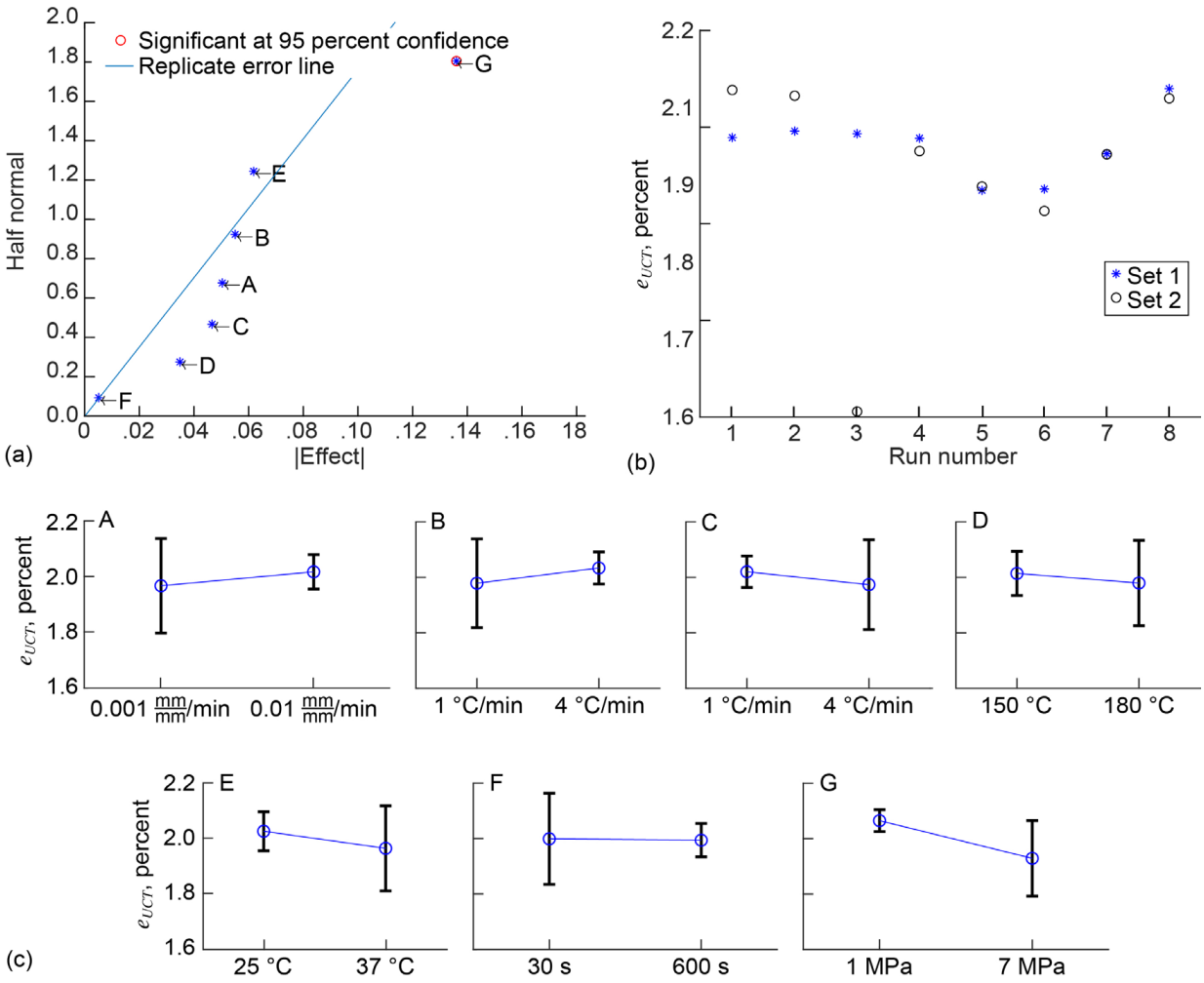

Figure 28.—Data, function of run number, and mean and standard deviation (STDEV) as a function of low- and high-level settings for strain at upper cycle temperature (after full thermal cycle under load), e_{UCT}. (a) Half-normal plot. (b) Function of run number for two replicates. (c) Mean and STDEV for A, strain rate; B, cooling rate; C, heating rate; D, upper cycle temperature (*UCT*); E, lower cycle temperature (*LCT*); F, hold time; and G, minimum load.

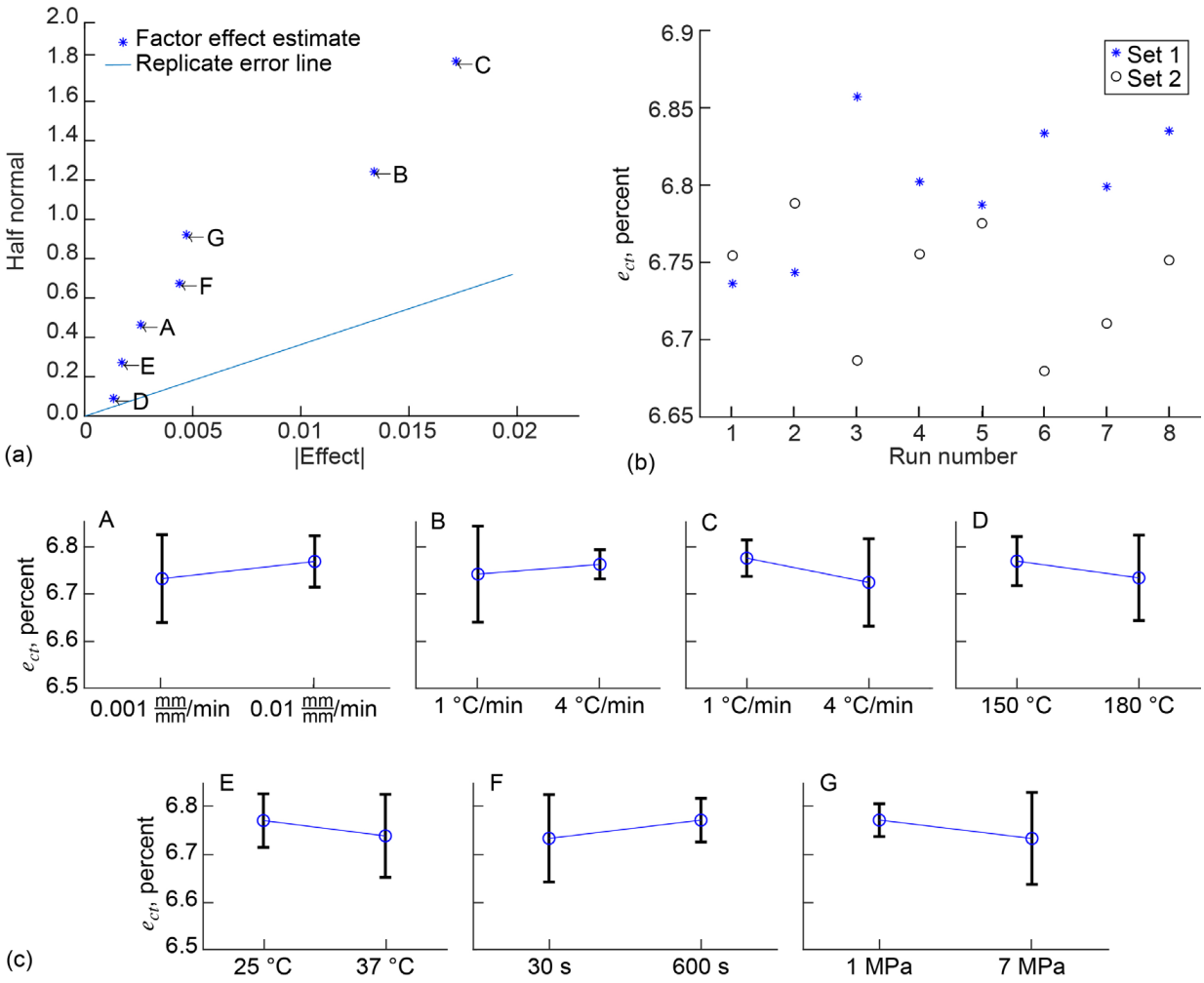

Figure 29.—Data, function of run number, and mean and standard deviation (STDEV) as a function of low- and high-level settings for cooling transformation strain, e_{ct}. (a) Half-normal plot. (b) Function of run number for two replicates. (c) Mean and STDEV for A, strain rate; B, cooling rate; C, heating rate; D, upper cycle temperature (*UCT*); E, lower cycle temperature (*LCT*); F, hold time; and G, minimum load.

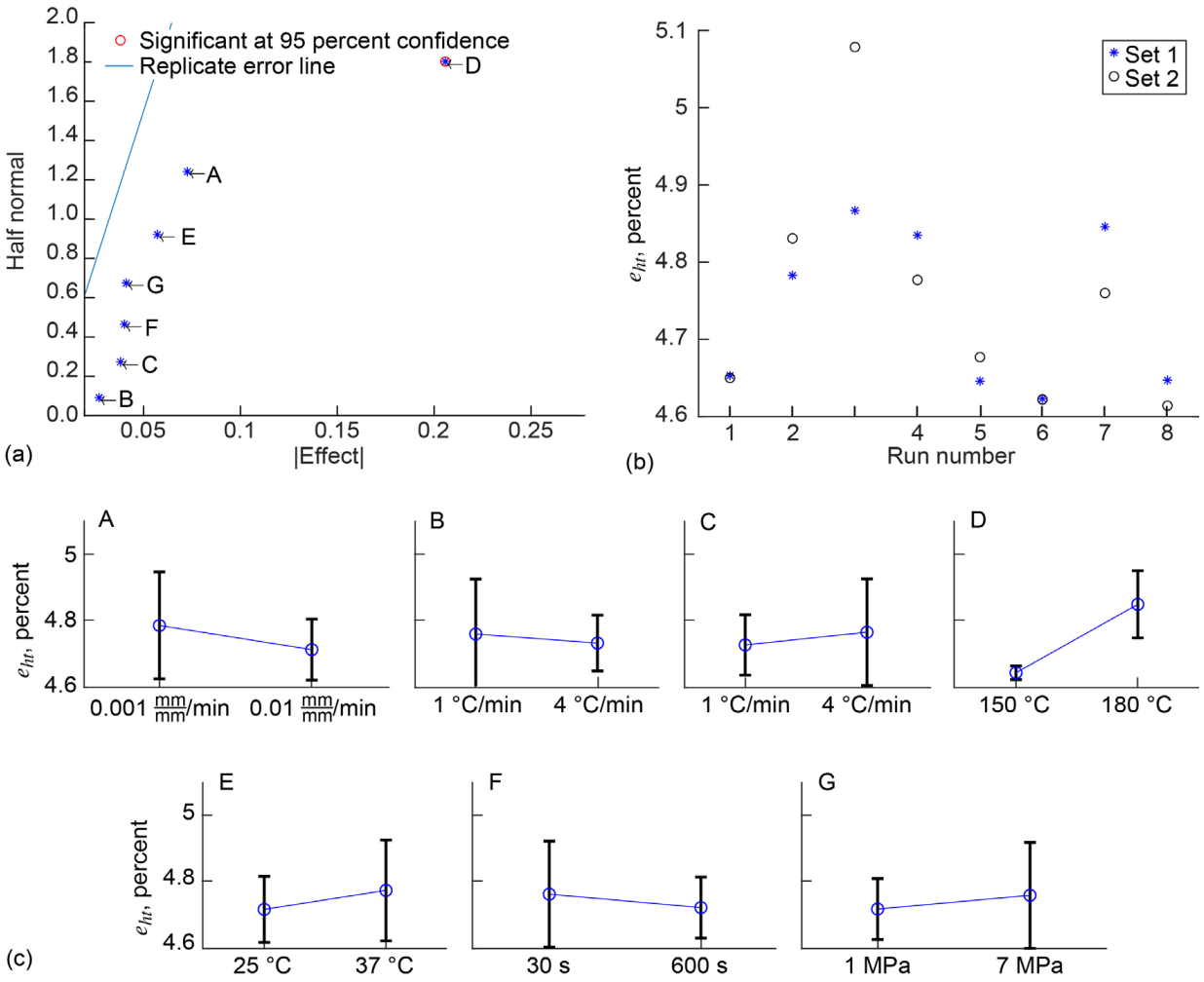

Figure 30.—Data, function of run number, and mean and standard deviation (STDEV) as a function of low- and high-level settings for heating transformation strain, e_{ht}. (a) Half-normal plot. (b) Function of run number for two replicates. (c) Mean and STDEV for A, strain rate; B, cooling rate; C, heating rate; D, upper cycle temperature (*UCT*); E, lower cycle temperature (*LCT*); F, hold time; and G, minimum load.

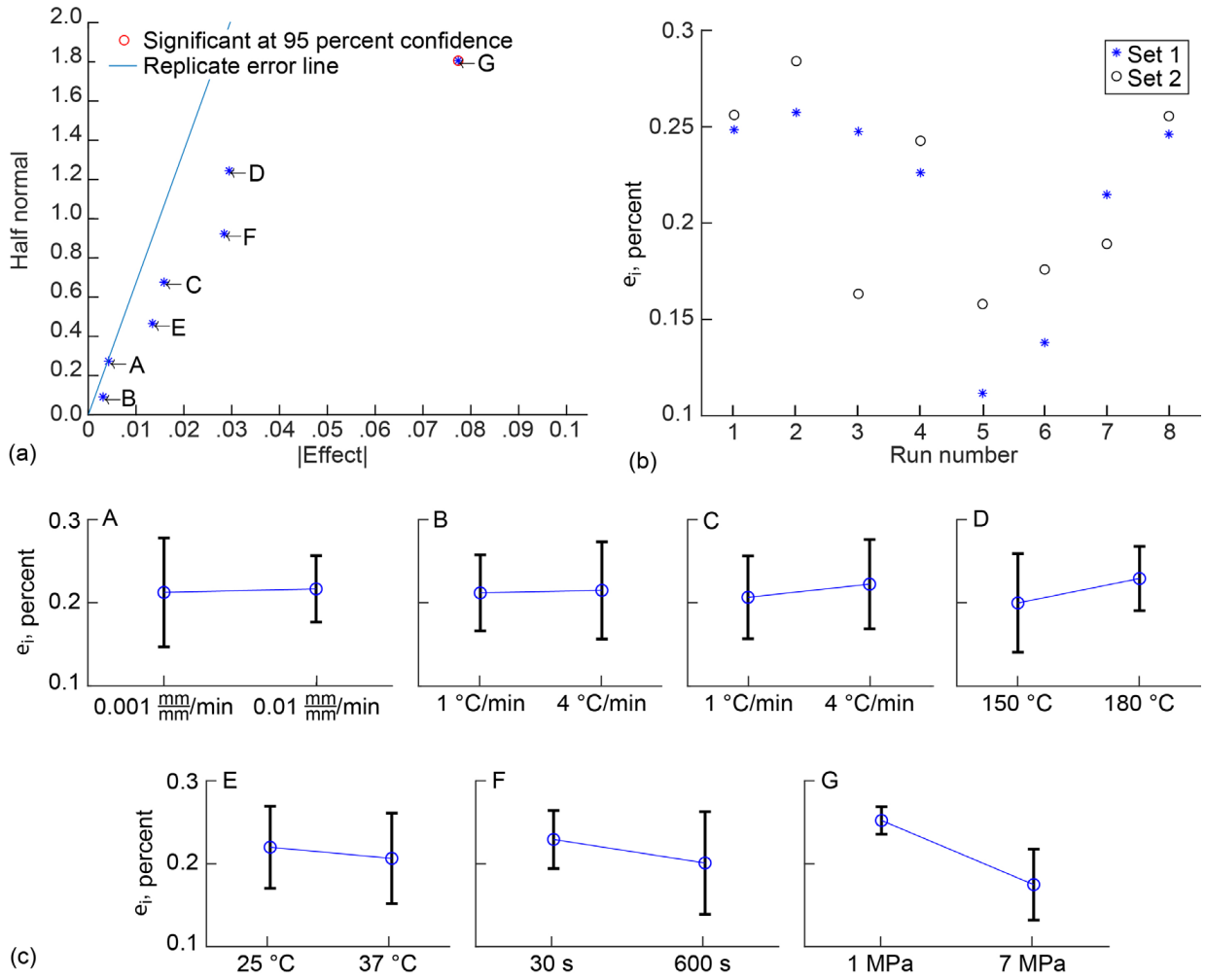

Figure 31.—Data, function of run number, and mean and standard deviation (STDEV) as a function of low- and high-level settings for initial loading strain (at upper cycle temperature (*UCT*), at load), e_i. (a) Half-normal plot. (b) Function of run number for two replicates. (c) Mean and STDEV for A, strain rate; B, cooling rate; C, heating rate; D, *UCT*; E, lower cycle temperature (*LCT*); F, hold time; and G, minimum load.

TABLE IV.—LIST OF RESULT VARIABLES SIGNIFICANTLY AFFECTED BY EACH FACTOR
[Numbers in parenthesis indicate importance ranking of factor for that result variable; that is, A_f (2nd) means given factor had second greatest effect on A_f.]

Factor	Effect of high level versus low level								
Strain rate, $\dot{e}$	Result variable	A_f[a] (3rd)	----------	----------	----------	---------	---------	----------	---------
	Effect	1.196	----------	----------	----------	---------	---------	----------	---------
Cooling rate, $\dot{T}_{cool}$	Result variable	A_s[b] (1st)	A_f*[c] (2nd)	A_f (1st)	----------	---------	---------	----------	---------
	Effect	1.902	1.825	–1.787	----------	---------	---------	----------	---------
Heating rate, $\dot{T}_{heat}$	Result variable	A_f (2nd)	----------	----------	----------	---------	---------	----------	---------
	Effect	–1.510	----------	----------	----------	---------	---------	----------	---------
Upper cycle temperature, *UCT*	Result variable	A_f* (1st)	M_s*[d] (1st)	e_{Af}[e] (1st)	e_{ht}[f](1st)	---------	---------	----------	---------
	Effect	17.300	3.713	–0.207	0.206	---------	---------	----------	---------
Lower cycle temperature, *LCT*	Result variable	M_f*[g] (1st)	----------	----------	----------	---------	---------	----------	---------
	Effect	2.000	----------	----------	----------	---------	---------	----------	---------
Hold time, t_{hold}	Result variable	----------	----------	----------	----------	---------	---------	----------	---------
	Effect	----------	----------	----------	----------	---------	---------	----------	---------
Minimum load, F_{min}	Result variable	A_f* (3rd)	e_{UCT}[h] (1st)	e_{Mf}[i] (1st)	e_{LCT}[j] (1st)	e_{As}[k] (1st)	A_f (4th)	e_{Ms}[l] (1st)	e_i[m] (1st)
	Effect	–1.675	–0.136	–0.119	–0.096	–0.090	–0.882	–0.081	–0.077

[a]Austenite finish.
[b]Austenite start.
[c]Austenite finish tangent line and data intersect.
[d]Martensite start tangent line and data intersect.
[e]Strain at austenite finish temperature (fit line intersection point).
[f]Heating transformation strain.
[g]Martensite finish tangent line and data intersect.
[h]Strain at upper cycle temperature (*UCT*) (after full thermal cycle under load).
[i]Strain at martensite finish temperature (fit line intersection point).
[j]Strain at lower cycle temperature (after cooling under load).
[k]Strain at austenite start temperature (fit line intersection point).
[l]Strain at martensite start temperature (fit line intersection point).
[m]Initial loading strain (at *UCT*, at load).

A list of all result variables found to be significantly affected by each factor as well as the associated half-normal ranking for each result variable are shown in Table IV.

5.0 Discussions

The seven selected factors were deemed to be the most likely factors to affect the UCFTC test outcome, and their impact on each result variable is outlined in the previously presented data. It should be restated that the tests presented here are only a portion of the overall ruggedness evaluation as it does not consider other geometries, other SMAs, or other testing organizations, nor does it account for variations due to operator analysis (fit) technique. It is also noted that the experiments performed comprise only a fractional factorial, and lack a foldover replicate to identify if the combination of any factors confound results. Additionally, the observed statistical significance of a factor does not completely confirm nor deny a physical, material effect on the selected alloy system studied, merely the presence of an observed effect in this experiment. Further testing is required to verify the mechanisms and nature of the effects seen.

The effects of strain rates on transformation parameters have been investigated extensively in constant-temperature, pseudoelastic conditions (Refs. 13 and 14), but little work exists detailing the effects of strain rate on thermally induced transformation. Given that the loading and unloading is taking place at only the *UCT* (austenite phase) and it is expected that the 100-MPa stress is still within the elastic portion of the material response, the strain rate should have a minimal effect. The rest of the test method is based on maintaining the stress at a constant level where the strain rates are no longer a factor. From Table III, it is shown that the strain rates have a minimal effect on the A_f by ~1.2 °C, which can be considered a minimally important factor in the UCFTC test method.

Heating and cooling rates have been previously reported to influence the transformation temperatures of NiTi and NiTiCu alloys measured by DSC (Refs. 15 and 16), but as with many rate-dependent phenomena in SMAs, the exact mechanism is not fully understood. Referring to Table IV, the heating and cooling rates mainly impacted the transformation temperatures (A_s, A_f, and A_f*) by no more than ~1.9 °C. The results indicated a decrease in A_f and increase in A_s from a –1 to –4 °C/min cooling rate and a decrease of A_f from a +1 to +4 °C/min heating rate. Although the impact is minimal, the austenite temperatures, A_f in particular, are found to be the most sensitive to heating and cooling rate compared to other parameters.

Though varying *UCT* has been previously shown to have significant effects on actuator hysteresis and transformation temperatures (Ref. 17), the large effect of *UCT* on A_f* and M_s* is likely due to the lower *UCT* setting of 150 °C being placed too low for a tangent line to be fitted accurately to the linear austenite (or high-temperature) region, providing a necessarily different fit between low- and high-*UCT* values. For the high-*UCT* case, there is a larger linear region in the austenite, allowing for a more accurate fit to the fully transformed austenite, and therefore a better measurement of the austenite coefficient of thermal expansion (CTE) slope, whereas for the lower *UCT* case, there is some small amount of transformation still occurring at *UCT*, which is reflected in the slope of the fit line. Figure 32 illustrates this discrepancy in fits and how it is likely responsible for *UCT*'s effect on e_{Af} as well. Note that any factor that affects e_{Af} or e_{As} individually, and not together, will necessarily affect e_{ht} to the same degree (recalling $e_{ht} = e_{As} - e_{Af}$), explaining the effect on e_{ht}.

Similar to *UCT*, the effects of *LCT* are likely related to tangent line fitting and do not suggest any significant material property variation as there is only a significant effect on M_f*, and not M_f or e_{Mf}. In the low-*LCT* case, there is a greater linear martensite region present at temperatures below the transformation, allowing a better fit to the martensite, and therefore a lower slope. Thus, it is unsurprising that a fit line would be more likely to intersect the data farther to the left (at lower temperatures).

Minimum load shows a significant influence on a wide variety of result variables, most of which are strains. The negative influence on such a wide variety of strains, occurring across the entire temperature range of the UCFTC test, suggests that higher minimum load during normalization shifts the entire hysteresis loop in the subsequent loaded cycle downward in the strain-temperature space, affecting the strain (Figure 33). Regardless of the mechanism of this effect, the primary understanding gained is that load applied during normalization heating has little effect on the material's actuation strains, as long as it is maintained below some nominal level (7 MPa for this study), but will likely alter the positioning of some transformation temperatures and their associated strains.

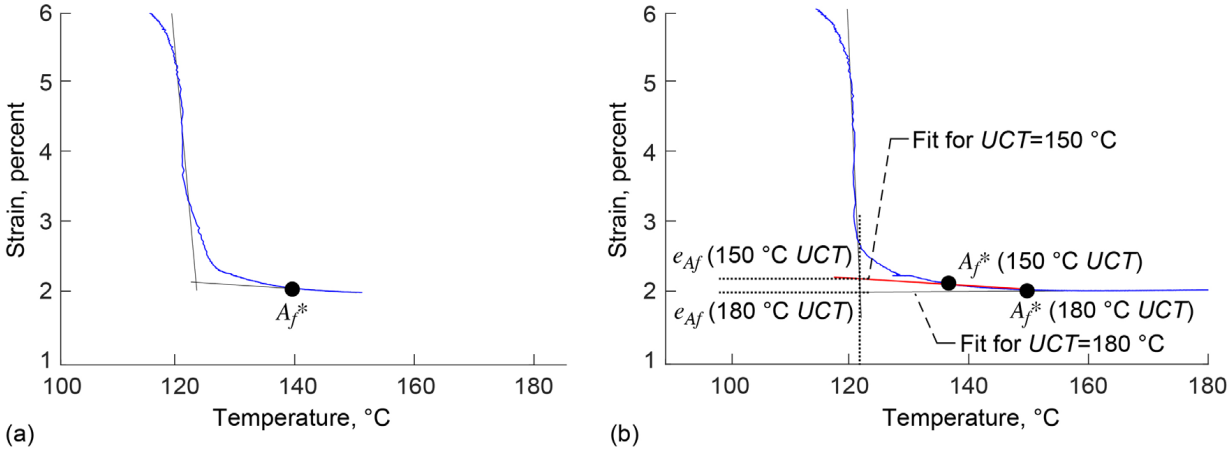

Figure 32.—Heating curves of runs 1 and 2, illustrating effect of upper cycle temperature (*UCT*) on transformation temperature fit lines.

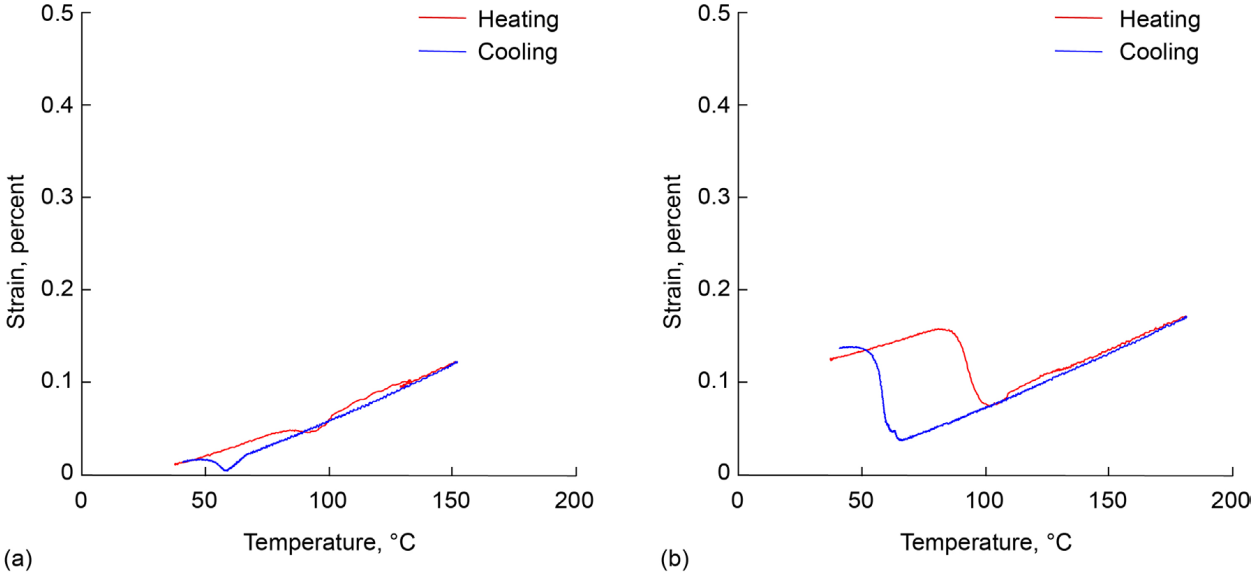

Figure 33.—Representative normalization curves. (a) G, minimum load setting of (–1). (b) G, minimum load setting of (+1).

6.0 Concluding Remarks

While vendors and test laboratories may use rates and limits outside of these presented here (after ensuring that they still obtain accurate results), this work was performed by using test factors and levels that should be sufficiently moderate to ensure good repeatability and accurate measurement of results for samples using the uniaxial constant force thermal cycling (UCFTC) test. For all factors, the magnitude of effect observed, even when statistically significant, was generally very minimal. Given that effects are specified in the units of the result variable observed (either °C or percent strain), the most significant effects shown in this work are relatively low compared to the differences frequently observed simply between two different analysts selecting linear fits to the same data to calculate transformation temperatures and strains. A difference in average A_s of 1.9 °C, for instance, while noteworthy, is not a critical change for most application purposes.

Most importantly, if a UCFTC test is performed in such a way that the entire transformation, including linear regimes in martensite and austenite, is obtained, the results of such a test are likely to be sufficiently rugged to variations in the testing factors evaluated in this experiment. Though a number of parameters may slightly change with testing factors such as temperature rates, strain rate, or minimum load, overall, the UCFTC test shows a commendable ruggedness to the factors tested in this work.

Additional work is warranted to evaluate the effect of geometry (e.g., wire, sheet, and rods), material lot (R-phase containing alloys and high-temperature alloys), analysis tools (e.g., during tangent line fitting), and other factors such as change in heating methods or loading equipment.

Appendix A.—Nomenclature

AVSI	Aerospace Vehicle Systems Institute
CASMART	Consortium for the Advancement of Shape Memory Alloy Research and Technology
CTE	coefficient of thermal expansion
DSC	differential scanning calorimetry
LeRCIP	Lewis' Educational and Research Collaborative Internship Project
SMA	shape memory alloy
STDEV	standard deviation
UCFTC	uniaxial constant force thermal cycling

Symbols

Ave	average results
A_{50}	austenite 50 percent = $(A_f + A_s)/2$
A_f	austenite finish
A_f*	austenite finish tangent line/data intersect
A_s	austenite start
A_s*	austenite start tangent line/data intersect
e	strain
$\dot{e}$	strain rate
effect	error of an effect
e_0	initial strain (at upper cycle temperature after normalizing)
e_{act}	actuation strain = $e_{LCT} - e_{UCT}$
e_{Af}	strain at austenite finish temperature (fit line intersection point)
e_{As}	strain at austenite start temperature (fit line intersection point)
e_{ct}	cooling transformation strain = $e_{Mf} - e_{Ms}$
e_{ht}	heating transformation strain = $e_{As} - e_{Af}$
e_i	initial loading strain (at *UCT*, at load)
e_{LCT}	strain at lower cycle temperature (after cooling under load)
e_{Mf}	strain at martensite finish temperature (fit line intersection point)
e_{Ms}	strain at martensite start temperature (fit line intersection point)
e_{res}	residual strain = $e_{UCT} - e_i$
e_{UCT}	strain at upper cycle temperature (after full thermal cycle under load)
F_{min}	minimum load
HWIDTH	hysteresis width = $A_{50} - M_{50}$
$I_x(z,w)$	incomplete beta function
LCT	lower cycle temperature
M_{50}	martensite 50 percent = $(M_f + M_s)/2$
M_f	martensite finish
M_f*	martensite finish tangent line and data intersect
M_s	martensite start
M_s*	martensite start tangent line and data intersect
N	number of runs
p	probability
reps	number of replicates
R_f	R-phase finish

R_f*	R-phase finish tangent line and data intersect
R_s	R-phase start
R_s*	R-phase start tangent line and data intersect
s_d	standard deviation of differences between replicates 1 and 2
s_{rep}	estimated standard deviation of test results
S_{effect}	standard error of an effect
T	temperature
t	Student's t-value (see Ref. 10)
$\dot{T}_{cool}$	cooling rate
$\dot{T}_{heat}$	heating rate
t_{hold}	hold time
$TSPAN$	thermal transformation span = $A_f - M_f$
UCT	upper cycle temperature
ν	degrees of freedom

Appendix B.—Data Formats

This appendix contains representations of the standardized data format (Table V) and the raw data files (Table VI).

TABLE V.—STANDARDIZED DATA FORMAT AS DEFINED BY THE AEROSPACE VECHICLE SYSTEMS INSTITUTE (AVSI) TEAM PER ASTM E3097

1	Test type	Uniaxial constant force thermal cycling (UCFTC)
2	Test note	Ruggedness tests
3	Test date	January 10, 2018
4	Lab	NASA–GRC–SH38B
5	Operator	O. Benafan
6	Material	NiTi, heat no. 836441
7	Sample identification	No. 8
8	Material condition	Hot rolled and heat treated (annealed)
9	Specimen geometry	Cylindrical dogbone (Ø = 0.1515 in., gage L = 0.75 in.)
10	Lower cycle temperature (*LCT*)	25
11	Upper cycle temperature (*UCT*)	150
12	Austenite start (A_s), °C	117.645
13	Austenite finish (A_f), °C	123.546
14	Martensite start (M_s), °C	70.628
15	Martensite finish (M_f), °C	68.807
16	Austenite start strain, e_{As}	0.06846
17	Austenite finish strain, e_{Af}	0.02233
18	Martensite start strain, e_{Ms}	0.00186
19	Martensite finish strain, e_{Mf}	0.06937
20	Strain at *LCT*, e_{LCT}	0.07101
21	Strain at *UCT*, e_{UCT}	0.02094
22	Cooling transformation strain, e_{ct}	0.06751
23	Heating transformation strain, e_{ht}	0.04613
24	Heating and cooling method	Induction
25	Temperature uniformity, °C	~2
26	Heating rate, °C/min	1
27	Cooling rate, °C/min	1
28	Strain measurement method	Mechanical extensometer with alumina rods
29	Strain rate (mm/mm per min)	0.001
30	Hold time(s)	30
31	Minimum load, MPa	1
32	Applied stress, MPa	100
33	Initial strain, e_0	0
34	Initial loading strain, e_i	0.002554

TABLE V.—STANDARDIZED DATA FORMAT AS DEFINED BY THE AEROSPACE VECHICLE SYSTEMS INSTITUTE (AVSI) TEAM PER ASTM E3097

35	Actuation strain, e_{act}	0.05007
36	Residual strain, e_{res}	0.018386
37	Method for A_{50} and M_{50} determination	(High temp + low temp)/2
38	A_s*, °C	74.5
39	A_f*, °C	140.2
40	M_s*, °C	73.5
41	M_f*, °C	47.2
42	Austenite 50 percent (A_{50}), °C	120.5955
43	Martensite 50 percent (M_{50}), °C	69.7175
44	Hysteresis width (HWIDTH), °C	50.878
45	Thermal transformation span (TSPAN), °C	54.739
46	Known A_f, °C	96
47	Known A_s, °C	77
48	Known R_f*, °C	
49	Known R_s*, °C	
50	Known R_s, °C	
51	Known R_f, °C	
52	Known M_s, °C	67
53	Known M_f, °C	50
54	Comments	Known transformation temperatures via DSC
55	User defined	
56	User defined	
57	User defined	
58	*** end header ***	

TABLE VI.—RAW DATA FILES

59	seconds	Deg C	MPa	%	user defined	user defined	user defined
60	time	temperature	stress	strain	user defined	user defined	user defined
61	1.0060222	21.154736	0.69224936	–0.0092264			
62	2.0060222	21.017036	0.83598107	–0.007681			
63	3.0060222	21.200634	0.61255819	–0.009124			
64	4.0060222	21.200634	0.7916289	–0.0078791			

Appendix C.—Run Replicates

This appendix contains plots of the run replicates (Figure 34 and Figure 35).

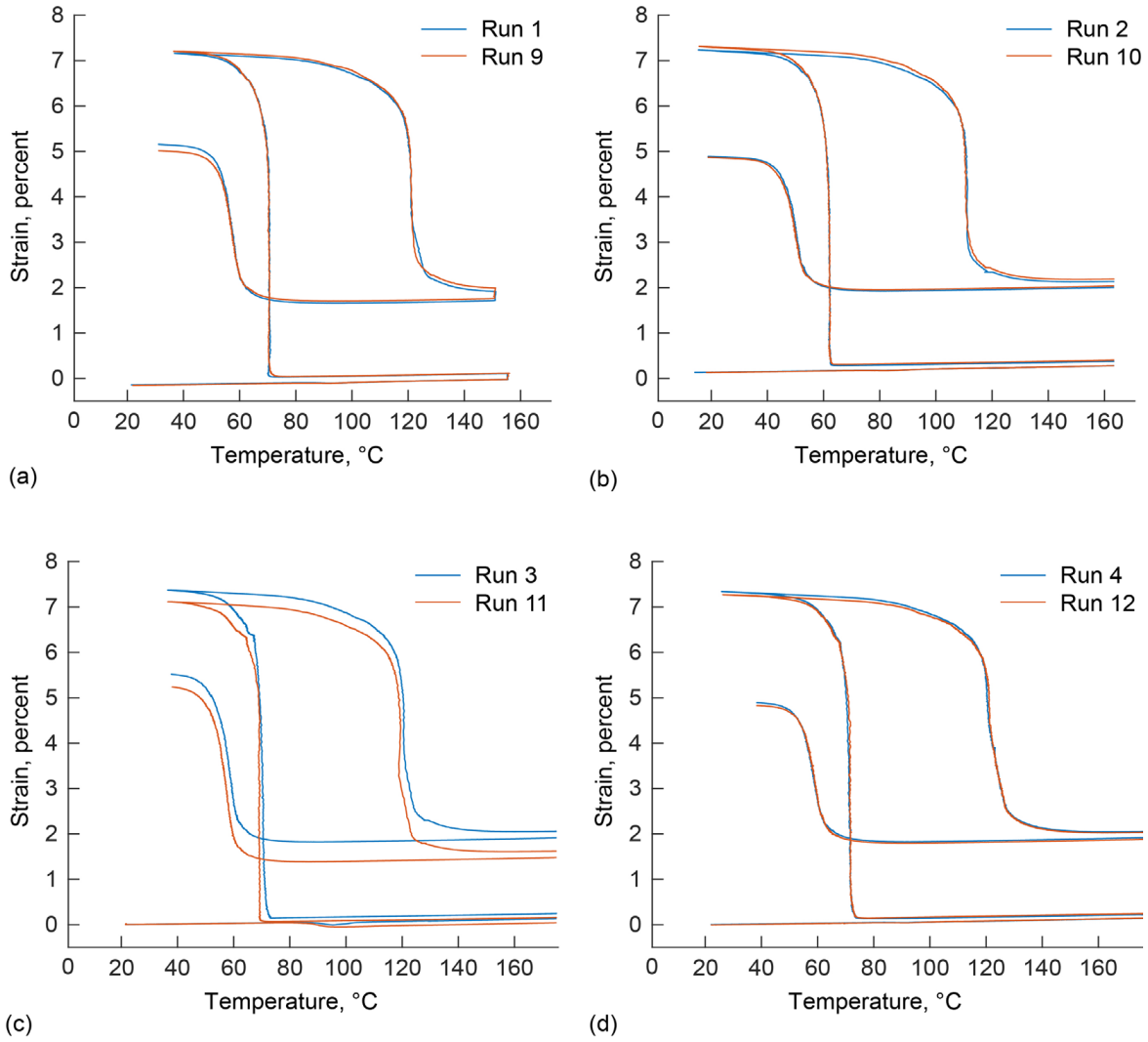

Figure 34.—Run replicate plots. (a) Runs 1 and 9. (b) Runs 2 and 10. (c) Runs 3 and 11. (d) Runs 4 and 12.

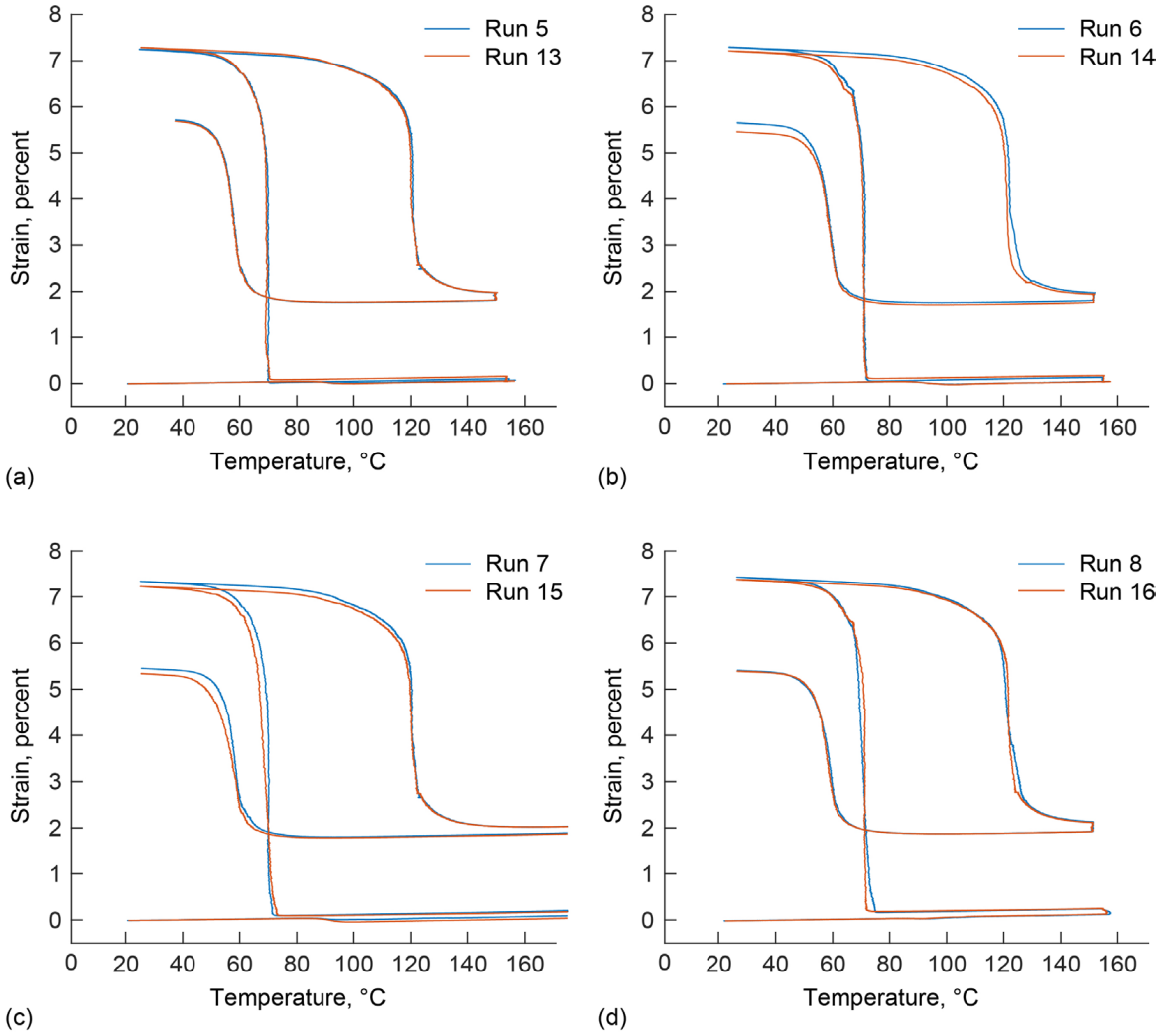

Figure 35.—Run replicate plots. (a) Runs 5 and 13. (b) Runs 6 and 14. (c) Runs 7 and 15. (d) Runs 8 and 16.

References

1. Benafan, O., et al.: Shape Memory Alloy Actuator Design: CASMART Collaborative Best Practices and Case Studies. Int. J. Mech. Mater. Des., vol. 10, no. 1, 2014, pp. 1–42.
2. Hartl, D.J., et al.: Standardization of Shape Memory Alloy Test Methods Toward Certification of Aerospace Applications. Smart Mater. Struct., vol. 24, 2015, pp. 082001–082006.
3. ASTM E3097–17: Standard Test Method for Mechanical Uniaxial Constant Force Thermal Cycling of Shape Memory Alloys. ASTM International, West Conshohocken, PA, 2017.
4. ASTM E3098–17: Standard Test Method for Mechanical Uniaxial Pre-strain and Thermal Free Recovery of Shape Memory Alloys. ASTM International, West Conshohocken, PA, 2017.
5. ASTM F2004–05: Standard Test Method for Transformation Temperature of Nickel-Titanium Alloys by Thermal Analysis. ASTM International, West Conshohocken, PA, 2010.
6. ASTM F2005–05: Standard Terminology for Nickel-Titanium Shape Memory Alloys. ASTM International, West Conshohocken, PA, 2015.
7. ASTM F2063–12: Standard Specification for Wrought Nickel-Titanium Shape Memory Alloys for Medical Devices and Surgical Implants. ASTM International, West Conshohocken, PA, 2012.
8. ASTM F2082–06: Standard Test Method for Determination of Transformation Temperature of Nickel-Titanium Shape Memory Alloys by Bend and Free Recovery (Withdrawn 2015). ASTM International, West Conshohocken, PA, 2006.
9. ASTM F2516–07: Standard Test Method for Tension Testing of Nickel-Titanium Superelastic Materials. ASTM International, West Conshohocken, PA, 2014.
10. ASTM E1169–17e1: Standard Practice for Conducting Ruggedness Tests. ASTM International, West Conshohocken, PA, 2017.
11. Bigelow, G.S., et al.: Shape Memory Alloy Analysis Tools. NASA Software, 2010.
12. Ko, Won-Seok; Grabowski, Blazej; and Neugebauer, Jörg: Development and Application of a Ni-Ti Interatomic Potential With High Predictive Accuracy of the Martensitic Phase Transition. Phys. Rev. B, vol. 92, 2015, p. 134107.
13. Grabe, C.; and Bruhns, O.T.: On the Viscous and Strain Rate Dependent Behavior of Polycrystalline NiTi. Int. J. Solids Struct., vol. 45, 2008, pp. 1876–1895.
14. Tobushi, Hisaaki, et al.: Influence of Strain Rate on Superelastic Properties of TiNi Shape Memory Alloy. Mech. Mater., vol. 30, 1998, pp. 141–150.
15. Nurveren, K.; Akdoğan, A.; and Huang, W.M.: Evolution of Transformation Characteristics With Heating/Cooling Rate in NiTi Shape Memory Alloys. J. Mater. Process. Technol., vol. 196, nos. 1–3, 2008, pp. 129–134.
16. Wang, Z.G.; Zu, X.T.; and Huo, Y.: Effect of Heating/Cooling Rate on the Transformation Temperatures in TiNiCu Shape Memory Alloys. Thermochim. Acta, vol. 436, nos. 1–2, 2005, pp. 153–155.
17. Padula II, S.A., et al.: Effect of Upper-Cycle Temperature on the Load-Biased, Strain-Temperature Response of NiTi. Metall. Mater. Trans. A, vol. 43, no. 12, 2012, pp. 4610–4621.